Observation of Intense Poynting Flux in the Dayside Cusp Region during Ion Outflows

A THESIS
SUBMITTED TO THE FACULTY OF THE GRADUATE SCHOOL
OF THE UNIVERSITY OF MINNESOTA
BY

Alyssa Hamre

IN PARTIAL FULFILLMENT OF THE REQUIREMENTS
FOR THE DEGREE OF
MASTER OF SCIENCE

Dr. John Wygant

June, 2011

Acknowledgements

I would like to thank my advisor, Dr. John Wygant, for all of his help with the research that I have done, both for his guidance of this project and for the amount of time that he has spent explaining and teaching me the concepts used in this work. In addition, thanks to Dr. Cindy Cattell and Dr. Tom Jones for reviewing the work presented here. A special thank you to Dr. Jack Scudder at the University of Iowa, who provided access to the Hydra particle data from Polar spacecraft used in this analysis. Additionally, I would like to acknowledge CDA web for the use of ACE/solar wind data. I could not have done this without help from and discussion with those in the University of Minnesota space physics group: Scott Thaller, Adam Hupach, Jesse Woodroffe, Lynn B. Wilson III, Dai Lei, Xiangwei Tang, Yan Yin, Kris Kersten, Aaron Breneman, John Dombeck, and Yan Song; in particular I would like to thank Scott Thaller for the use of his Poynting flux program, Jesse Woodroffe for his help with LaTeX formatting, and both Lynn Wilson and Dai Lai for their help with rotating data into the appropriate coordinate system.

Dedication

May the name of the Lord, who reigns over heaven and earth, be glorified in the work presented here.

To my family, for their continual support and encouragement to persevere through the difficult times, and for their love and caring that have uplifted me time and time again.

To my grandpa Bill Hamre, B.K., and D.L., for believing that I could do this, even before I did; and to E. D., who helped me to have endurance through grad school.

To my students, who have given me hope.

Soli Deo Gloria.

Abstract

Polar spacecraft data was used to take inventory of the different wave and particle energy forms present in the dayside intermediate-altitude cusp region during periods of intense Poynting flux seen in the major geomagnetic storms in October and November 2003. From this inventory, the energy budget of this region during northward and southward IMF was inferred. Dominant forms of energy in this region include Poynting flux in three frequency bands, large upgoing ion fluxes, and energetic particle fluxes perpendicular to the magnetic field. Hydra particle data from Polar showed outflowing ions with high energies simultaneous to intense Poynting flux. Filtering the Poynting flux over three time scales revealed that only the energy from the low-frequency Poynting flux is consistently sufficient to account for the ion kinetic energy flux seen during these intervals. The presence of field-aligned current structures in the magnetic field data suggests that the low-frequency Poynting flux associated with these structures may be powering the energization of upgoing ions. The electric and magnetic field data were used to detect Alfven waves, and Alfvenic Poynting flux is consistently another of the important forms of energy present. Moderate fluxes of ions energized perpendicular to the magnetic field (as seen in the Hydra data) may be indicative of ion cyclotron or kinetic Alfven waves heating the ions perpendicular to the field.

Contents

List of Tables

List of Figures

Chapter 1

Introduction

One of the most crucial issues in space physics is that of energy transfer resulting from the interaction between the solar wind and the earth's magnetic field. Taking inventory of the different types of energy associated with this process is an important step in understanding magnetic reconnection and its effects. Since reconnection occurs universally, including on the sun, at other planets within the solar system, and on extra-galactic objects such as neutron stars, work to understand reconnection is applicable not only in the earth's magnetosphere but also on a larger scale.

The work presented here will be examining particle and wave energy in the earth's dayside cusp region at intermediate altitude (approximately $2R_E$ to $4R_E$) during geomagnetic storms using Polar spacecraft data. A representation of the spacecraft passing through the cusp region is presented in Figure 1.1. Because the cusp is directly connected to the interaction between the solar wind and the magnetosphere that occurs in the subsolar region or at high latitudes, analysis of the energy budget in the cusp provides insight into the reconnection process at these locations, which is more clearly shown in Figure 2.2. Examining this region during geomagnetic storms allows the detection of the processes which occur when the magnetosphere is being most strongly driven. By studying the energy budget at a low enough altitude, it is possible to detect the different forms of energy present shortly before they are dissipated in the ionosphere. However, Polar is still at a high enough altitude to provide a different perspective on the types of energy present than that obtained by near-Earth spacecraft such as FAST. Additionally, Polar has an advantage over FAST that it can still detect a significant

portion of the particles which magnetically mirror above FAST. The specific types of energy that may be present in the cusp will be further expanded upon in the background section of this work.

It is the intent of this study to explore the energy in the cusp in order to provide an estimate of how much energy is flowing into and away from the earth's ionosphere, and to delineate into what forms this energy is partitioned. The exploration of these issues will be presented in the manner indicated below.

- Chapter 2 briefly explains the background science and previous work relevant to this study.
- Chapter 3 contains an explanation of the spacecraft and instrumentation used to obtain data.
- Chapter 4 describes the criteria used to select events included in the study and how data for these events was analyzed.
- In Chapter 5, the data for a large Poynting flux event during northward IMF on November 4^{th}, 2003 is presented.
- Chapter 6 presents similar data, again during northward IMF, for an event on October 31^{st}, 2003.
- Chapter 7 presents data for an event on November 20^{th}, 2003, which is during southward IMF, but otherwise is similar to the previous two events.
- In Chapter 8, the data for the three events shown in Chapters 5-7 is analyzed and compared.
- Chapter 9 concludes the thesis with an overview of the analysis presented and motivating questions for further research.

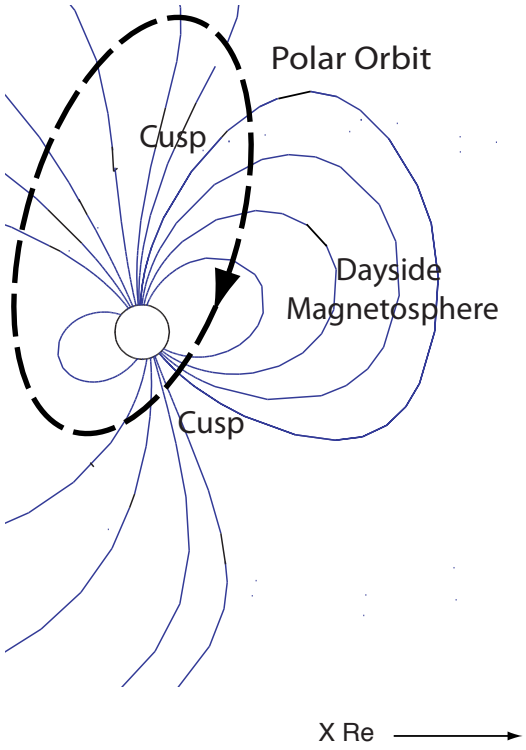

Figure 1.1: The diagram above shows a schematic of the trajectory of Polar spacecraft through the magnetosphere, with the arrow at the bottom indicating the positive x-direction towards the Sun. The magnetosphere structure is taken from a diagram in P.J. Cargill et al. 2005 [12].

Chapter 2

Background

Magnetic reconnection is a phenomenom in which the re-configuration of magnetic field lines causes an explosive release of energy [2]. One of the many locations in which this occurs is the sub-solar region, at which reconnection takes place between the Interplanetary Magnetic Field (IMF) and the geomagnetic field [2]. The reconnection process in this region differs depending on the orientation of the IMF. When examining the IMF, GSM coordinates are often used, in which the z-direction is parallel to the Earth's magnetic dipole axis, the x-direction points toward the sun, and the y-direction is perpendicular to the x and z directions [17]. GSE coordinates are also used, in which the x-direction is the same as for GSM, but the z-direction is perpendicular to the ecliptic plane and the y-direction lies in the ecliptic plane and points toward dusk [17]. The z-component of the IMF magnetic field is used to define when the IMF is "southward" (has a negative z-component) and "northward" (has a positive z-component).

If the IMF is pointed strongly southward, reconnection occurs on the dayside magnetopause, where the Earth's dipolar magnetic field points north [2]. If the IMF is pointed northwards, reconnection may instead occur on the nightside near the poles at oppositely-directed field lines in a region known as the cusp [18]. In both cases, the reconnected field lines map to the cusp region, which is the boundary between open (reconnected) and closed (dipolar) field lines. Figure 2.2 shows a schematic of reconnection in the subsolar region for southward IMF with convection toward the tail (left diagram) and at high latitudes for northward IMF with convection toward the magnetopause (right diagram).

Reconnecting field lines mapping to the cusp cause both solar wind plasma and parallel-propagating waves excited by the reconnection process to travel along these field lines toward the Earth. Since the reconnection process is not well understood, assessing the energy balance of the cusp will provide important information about what processes may be driven as a result of reconnection.

There are a variety of different forms of energy related to reconnection. Most directly, ion jets flow away from the reconnection region, causing energetic particles to stream towards the earth's ionosphere. Reconnection may also cause oscillations along the field lines in the form of Alfven waves. The presence of Alfven waves is often associated with the flow of energy in the form of Poynting flux along field lines toward the earth. In addition, the large-scale convection of magnetic field lines sets up a field-aligned current system, which is also a possible source of Poynting flux. At lower altitudes, the field-aligned currents may set up electric fields parallel to the magnetic field, causing particle acceleration along the field lines. Both ion cyclotron waves and kinetic Alfven waves present at low altitudes may heat ions perpendicular to the field, causing the presence of perpendicular ion energy fluxes. Conservation of the first adiabatic invariant, given by $\mu = \frac{mv_\perp{}^2}{2B}$, and conservation of energy, $E = \frac{1}{2}mv_\perp{}^2 + \frac{1}{2}mv_\parallel{}^2$, causes these particles to experience the magnetic mirror force, such that they will mirror near the earth and stream away from the earth along magnetic field lines [17]. This contributes another energetic particle population in addition to those from jets or energized by the field-aligned current system. A general schematic of the energy forms can be seen in Figure 2.1. In addition to finding what forms of energy are present in the cusp, the comparison of the Poynting flux energy to the particle energy is of interest. In this work, Poynting flux is divided into three frequency bands, including a high frequency band which is expected to be roughly Alfvenic, low-frequency which is associated with field-aligned current structures, and medium-frequency (between the other two bands) to make sure that the majority of the Poynting flux energy is being accounted for. Chaston et al. (2005) examines particle energization in the forms of parallel electron acceleration, transverse ion acceleration, and Joule heating; in this work, these catagories of energetic particles will be addressed with the exception of Joule heating [1].

Though not specifically related to energization, one phenomenon that can be seen clearly in the cusp regions is the velocity filter effect of the particles streaming down

convecting field lines [18]. Velocity filtering occurs when charged particles moving at different velocities parallel to the magnetic field arrive at the atmosphere at different times as a result of the presence of large-scale electric and magnetic fields, causing $\frac{\vec{E}\times\vec{B}}{B^2}$ drift. Since the $\frac{\vec{E}\times\vec{B}}{B^2}$ drift is perpendicular to the field line, particles with smaller velocities parallel to the field line will have a longer time to drift, whereas higher-energy particles will have less time to drift. This results in a population with either increasing or decreasing energy with latitude, visible on energy spectrum plots. Different directions of the convection electric field, which is dependent on the z-component of the IMF, will cause a reversal of this signature. Precipitating ions are expected to decrease in energy with latitude for southward IMF, whereas they will increase in energy with latitude for a northward IMF [18].

One of the phenomena of interest that will be presented in the events discussed is that of upgoing ion fluxes. The 1999 work by Moore et al. suggested that dense, cold ionospheric outflows were a result of the polar ionospheric plasma responding to incident Coronal Mass Ejection (CME) magnetic clouds [14]. This outflow would then travel away from the earth near the cusp and out to the near-Earth plasma sheet [14]. McFadden et al. (2001) also proposed that the ion outflows from the cusp would go into the tail, as opposed to the polar cap boundary ion outflows, which would instead flow into the ionospheric plasma [7]. The 2005 paper by Strangeway et al. provided clarity on the issue of ion outflows by using FAST spacecraft data for the September 24-25, 1998 storm on the Earth's dayside [13]. The two sources for ion outflow that they proposed were ion heating from frictional dissipation of downward Poynting flux and electron heating from soft (less than 500eV) electron precipitation [13]. Both of these events take place in the cusp and were correlated with ion outflows, although neither process would heat the ions to an energy at which they could escape the ionosphere [13]. Instead, it was suggested that there is transverse wave heating which would energize the ions to the point that they could escape in the form of the observed ion outflows [13]. One possibility for the transverse heating necessary to energize the ions for escape would be dispersive Alfven waves, a mechanism proposed by Chaston et al. in 2004 in which the high-frequency dispersive Alfven waves provide rapid ion acceleration perpendicular to the field [3]. The final results of the Strangeway analysis are that both Poynting flux and soft electron precipitation were correlated with ion outflows, so neither source could

be eliminated as the cause [13]. Their results were confirmed by Zheng et al. (2005), who used Polar data to find that the dominant influences for field-aligned ion outflows were Poynting flux and precipitating electrons [15]. Note that both the Strangeway et al. (2005) and Zheng et al. (2005) studies use number flux of the outflowing ions, whereas this study uses kinetic energy flux [13], [15]. A rocket study published in 2010 by Burchill et al. also found an apparant link between precipitating electrons and ion upflows, in accordance with the Strangeway and Zheng papers [6]. In line with these studies, Polar data will be used in this work to examine the different forms of energy present simultaneous to ion outflows.

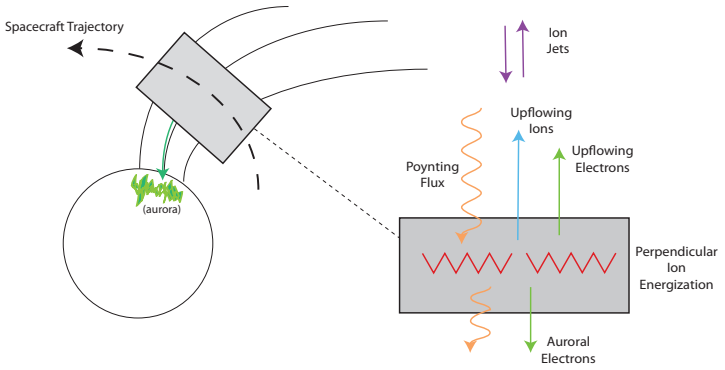

Figure 2.1: This shows a general schematic of the different forms of energy detected in the mid-altitude cusp region.

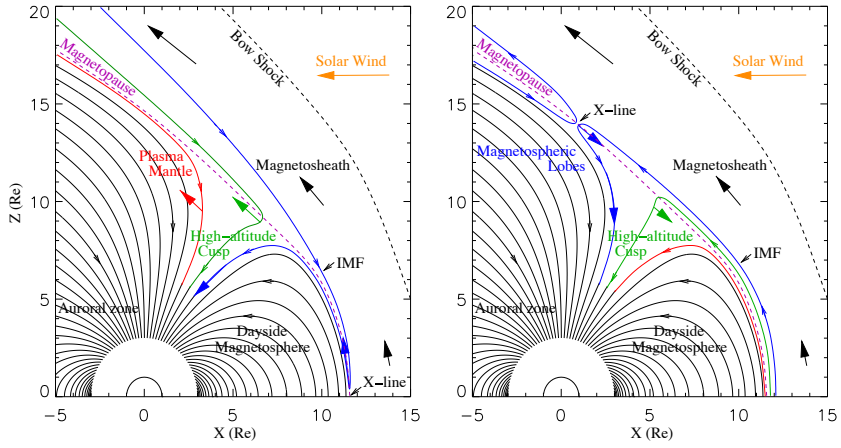

Figure 2.2: From P.J. Cargill et al. 2005 [12]. The blue line represents an IMF field line as it reconnects with the Earth's magnetic field, where the actual reconnection location is indicated by the X-line (labelled). The green field line shows a reconnected field line, and the green arrow indicates the convection direction of this field line. In the case of southward reconnection, the X-line is far in front of the Earth, then convects northward toward the cusp and over the pole (left diagram). By contrast, the northward scenario shows reconnection occuring tailward of the cusp, then convecting sunward towards the cusp (right diagram).

Chapter 3

Instrumentation

3.1 Polar

The main spacecraft used for this study was Polar spacecraft, which was designed to study the near-earth region of the magnetosphere, in particular the regions near the Earth's poles. Its orbit was highly elliptical, with perigee at a distance of 1.8 earth radii (R_E) and apogee at 9 R_E. At launch, the initial apogee was 20° from the North pole, and the orbit precessed 18° per year. The spacecraft was cylindrical, with four 65m wire antennae and two 5.5m axial booms which were used to make electric field measurements. In addition, two 6m booms held the DC magnetometer and the triaxial search coils used for measuring the magnetic field. In total, there were twelve instruments present on the spacecraft used to measure the electric and magnetic field, plasma density and composition, and take images. In order to keep the imaging instrument stable, the spacecraft had a de-spun platform.

This study focused on data from the electric field instrument, which allowed for the measurement of the full 3-dimensional vector field used to calculate the full Poynting flux. As mentioned above, there were two pairs of longer wire booms which are in the spin plane of the orbit, and a shorter pair along the spin axis, all of which had spherical sensors at the tips [11]. The three boom orientations make up the spacecraft coordinate system, as indicated in Figure 3.1. In orbit, the 56-direction is along the spin axis, the xy-direction is nearly in the ecliptic plane, and the z-direction is roughly along the magnetic pole. A measurement of the potential difference between the spheres and

the spacecraft was used to measure the electric field. The instrument was capable of measuring in a frequency range from DC to above 20kHz and an amplitude range from 0.02 to 1000 mV/m. Additionally, the electric field instrument was used to measure thermal electron density in the range of 0.01 to 100 $particles/cm^3$ [11]. High resolution data could be obtained and stored in the burst memory in the case of events with rapid field variations [11]. In addition, it is useful for this study that Polar spacecraft velocity was roughly 4 km/s, which is greater than the cusp velocity at this point, such that the data captured spatial structures while moving through the cusp.

Additional data was obtained from Polar's pair of triaxial fluxgate magnetometers [4]. The magnetometers were on a 6 meter boom and collected data at a rate of 9.2s in spacecraft coordinates and 0.92min. in GSE/GSM coordinates [4]. In addition, the magnetometers were also capable of taking data at a rate of 100 vectors/s for short periods of time [4]. Particle data was obtained from the Hydra plasma instrument, which sampled electrons and ions with time resolution of 0.5s and could detect particles in the energy range of 2eV to 35keV per particle [9]. Hydra also took a full sweep of particle energy distributions twice per spacecraft rotation. In additon, Hydra communicated with the electric field instrument such that either instrument could trigger a burst mode sampling [9].

3.2 ACE

The ACE (Advanced Composition Explorer) spacecraft was launched in 1997 for the purpose of examining the composition of the solar wind, interplanetary medium, interstellar medium, and galactic matter [5]. It was launched in August of 1997 and moved into orbit at the libration point of 240 R_E, with the instruments on the front of the spacecraft facing the sun. Using a variety of spectrometers, an ionic charge analyzer, a twin fluxgate magnetometer, and two electron-proton-alpha monitors, ACE can detect particles of a variety of masses with energies ranging from 1 keV to 500 MeV. In addition, the data taken from ACE provides real-time solar wind conditions, giving approximately 1 hour of warning before a geomagnetic storm arrives at the Earth [5]. In the work presented, ACE magnetometer and plasma instsrument data will be used in order to gauge the solar wind conditions during the events of interest.

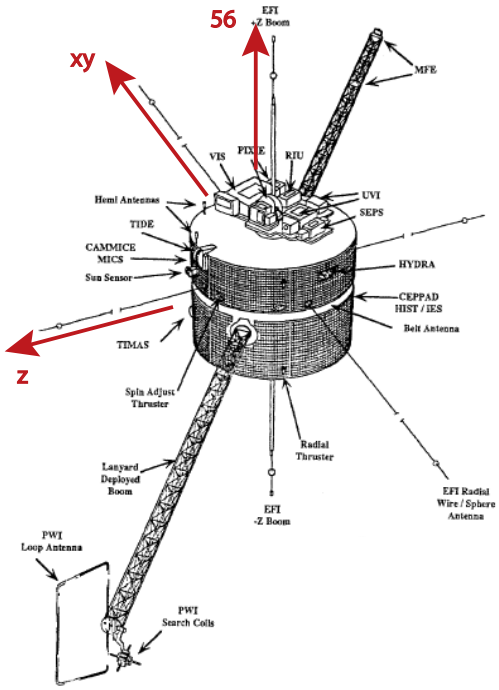

Figure 3.1: This is a general sketch of Polar spacecraft, modified from Harten and Clark (1995), with the spacecraft coordinate system indicated by the red arrows [16].

Chapter 4

Event Selection and Analysis Approach

4.1 Selection Criteria

The original intent of this work was to examine the Poynting flux seen by Polar on dayside intermediate-altitude passes during times of high solar activity and large geomagnetic storms. By examining the cusp during active times when the geomagnetic field is highly distorted and the reconnection process is most intense, the amount of energy flowing toward or away from the earth (as outlined in the Background section) will be most clearly distinct from any steady-state background energy forms. We focus on the most extreme geomagnetic storms recorded during the life of Polar, which took place in October and November of 2003. The presence of these storms can be ascertained by examining the Dst index as seen in panel (a) of Figures 4.1 and 4.2, which drops well below the -50nT definition of a geomagnetic storm in both cases, even to as low as -400nT in the November storm.

For the October storm, the beginning of the storm is visible on October 29th as the Dst drops to about -150nT, followed by very large drops on October 30th and 31st, as seen in panel (a). These drops are concurrent with peaks in AE shown in panel (b). The Dst stays mainly below 0nT for the days following, and drops again to roughly -70nT for a smaller storm on November 4th. As can be seen in panels (c) through (f), there is an absence of solar wind velocity and density data during the peak of the storm

from ACE spacecraft. Note that the ACE data (panels (c) through (h)) is not lagged to the magnetosphere in these plots, but that this lag is insignificant when examining data over this long of an interval. Peaks in the magnetic field magnitude and z-GSM component are seen in panels (g) and (h) simultaneous to the drops in Dst. These peaks are indicative of the arrival of the Coronal Mass Ejection (CME) magnetic cloud at the location of ACE.

The November storm is marked by the significant Dst drop mid-day on November 20th to roughly -425nT, as seen in panel (a). The recovery to above-storm level Dst takes until about halfway through November 23rd. As with the October storm, peaks in the AE mirror the drops in Dst, shown in panel (b). The magnitude of the x-GSE velocity increases sharply during the beginning of the Dst drop on November 20th, with smaller but similarly sharp fluctuations in the y- and z-components, as seen in panels (c) through (e). This increase in velocity also causes an increase in dynamic pressure, which affects how strongly the system is driven. Proton number density, in panel (f), increases roughly an order of magnitude over the value seen prior to the CME. The magnetic field magnitude and z-GSM component, shown in panels (g) and (h), peak at the same time as the drop in the Dst and again show the arrival of the CME magnetic cloud.

For the purposes of this work, "intermediate-altitude" was defined as when Polar was at a distance between 1.75-4R_E. In order to ensure that a given pass was while Polar was on the day side, the magnetic local time (MLT) was constrained to be between 9 and 15. In addition, the data was constrained to time periods when Polar was at a high invariant latitude (ILAT), which was taken to be roughly 60° (magnitude) or greater. By examining data only at these high ILAT values, the intervals examined were most likely to include a pass through the cusp.

Data was examined for 10/29 through 11/04 and 11/20 through 11/23. Within these intervals, the times in which Polar met the aforementioned criteria (particularly the R_E and MLT constraints) were selected, and the high-frequency Poynting flux (using fields filtered 1-10s) was calculated for these events using the program described in the following section. From these events, those with large mapped Poynting flux were examined further in order to limit the focus to times when the energy flows are the largest. The events of interest are listed in Table 4.1.

Date	Time (UT)	R_E	MLT	ILAT (degrees)	Smag ($\frac{ergs}{cm^2 sec}$)
10/29/2003	10:57	2.9	9.4	-82.8	22
10/31/2003	18:06	2.9	10.2	-75.8	40
11/03/2003	00:51	2.1	9.5	-63.7	53
11/04/2003	14:21	3.5	8.8	-86.1	50
11/20/2003	15:47	2.2	8.0	-59.8	120
11/20/2003	15:51	2.3	8.1	-63.0	120
11/23/2003	18:00	3.5	10.1	-81.3	17

Table 4.1: List of events with strong Poynting flux for October and November 2003. Note that the Poynting flux values listed are mapped to the ionosphere, and are calculated using electric and magnetic field data smoothed over 1s and detrended over 10s.

4.2 Analysis Approach

The program used for the analysis of Polar data was originally written by Scott Thaller, with a few modifications made in order to customize the analysis to the events selected. The quantities used by the program included density, spacecraft potential, spacecraft velocity, and electric and magnetic field data. Anomalously large spikes in the magnetic field and the density data were removed, and all of the data was resampled to the data rate of the magnetic field. To account for spacecraft motion through the magnetic field, the $\vec{v} \times \vec{B}$ component of the electric field was subtracted from the electric field data.

In order to calculate the full Poynting flux, the 3-dimensional vector electric and magnetic field data was detrended (fluctuations below a certain period removed) and smoothed (fluctuations above a certain period removed), such that only fluctuations within a certain frequency range were present. The Poynting flux was then calculated with these filtered quantities using Equation 4.1.

$$\vec{S} = \frac{\delta\vec{E} \times \delta\vec{B}}{\mu_0} \tag{4.1}$$

To find the field-aligned Poynting flux, the Poynting flux was dotted into the direction of the magnetic field. When using the full three-dimensional electric field, the 56-axis data is less reliable due to measuring E with shorter booms. In order to check the validity of the full Poynting flux calculation, the Poynting flux was calculated using

just the xy and z electric field components. Additionally, the Poynting flux was also calculated by rotating the electric and magnetic field data into background magnetic field-aligned coordinates, then multiplying the a perpendicular electric field component by a perpendicular magnetic field component as another check that the Poynting flux calculation was valid. Locator quantities such as magnetic local time (MLT), invariant latitude (ILAT), and L-shell were calculated using the Tsyganenko 2004 model such that these quantities reflect a storm-distorted magnetic field. Note that if the ILAT values were less than zero, indicating the spacecraft position in the southern hemisphere, the sign of the Poynting flux was reversed such that positive Poynting flux is always earthward-flowing Poynting flux in the plots presented. The magnitude of the Poynting flux mapped to the ionosphere was calculated by multiplying the in-situ Poynting flux by the ratio of the magnetic field at the ionosphere to the background magnetic field at the spacecraft position.

4.2.1 Tsyganenko models

During quiet times, the Earth's magnetic field in the inner magnetosphere can be modelled as approximately dipolar. However, the field may be drastically distorted during storm times. The Tsyganenko 2004 model used in this work takes the time averages of the IMF and solar wind conditions over the hour preceding the time interval of interest and uses them to model the magnetosphere at the time of interest. Using averages over the preceding hour allows the magnetosphere model to have time to react to the new conditions, which accounts for current system reaction times. Tsyganenko's work demonstrated that the Dst calculated using this model correlated well with actual Dst measurements, so it is assumed to be sufficiently accurate for the data analysis presented here [20].

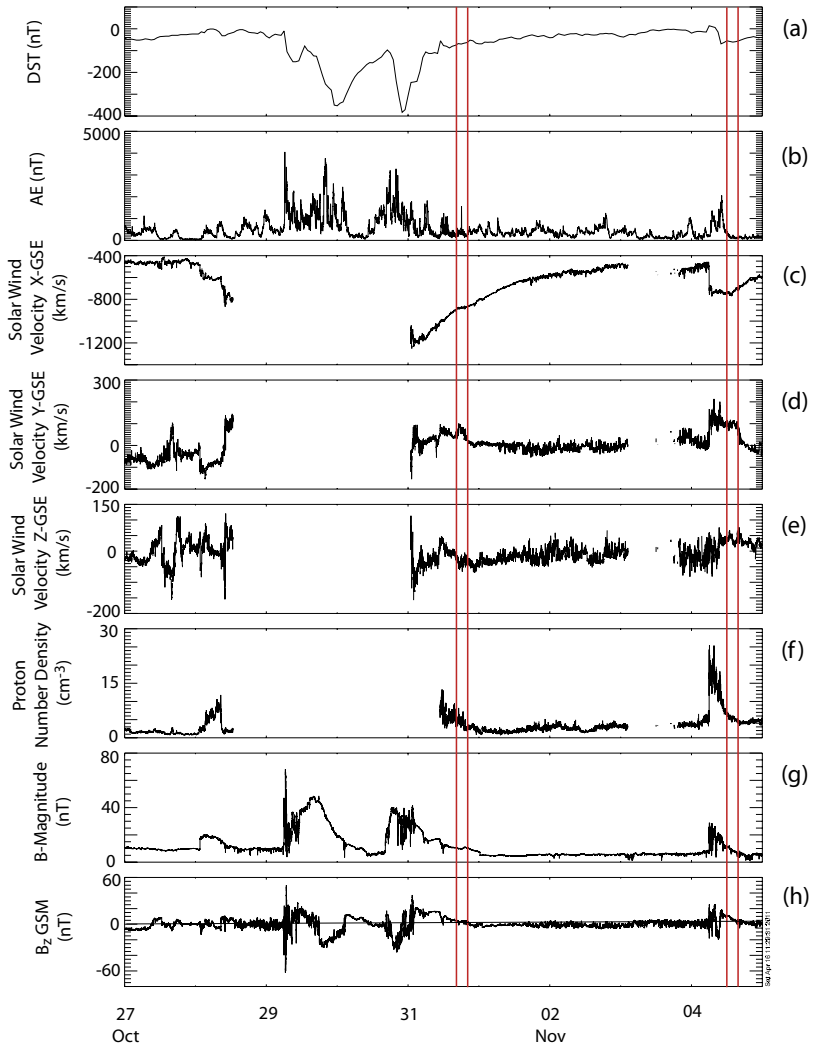

Figure 4.1: Solar wind conditions for the October 2003 storm are presented, including (a) Dst, (b) AE index, (c)-(e) solar wind velocity in GSE coordinates, (f) proton number density, (g) magnetic field magnitude, and (h) magnetic field z-GSM component surrounding the storm. The vertical red lines delineate the November 4 and October 31 passes presented in Chapters 5 and 6, respectively.

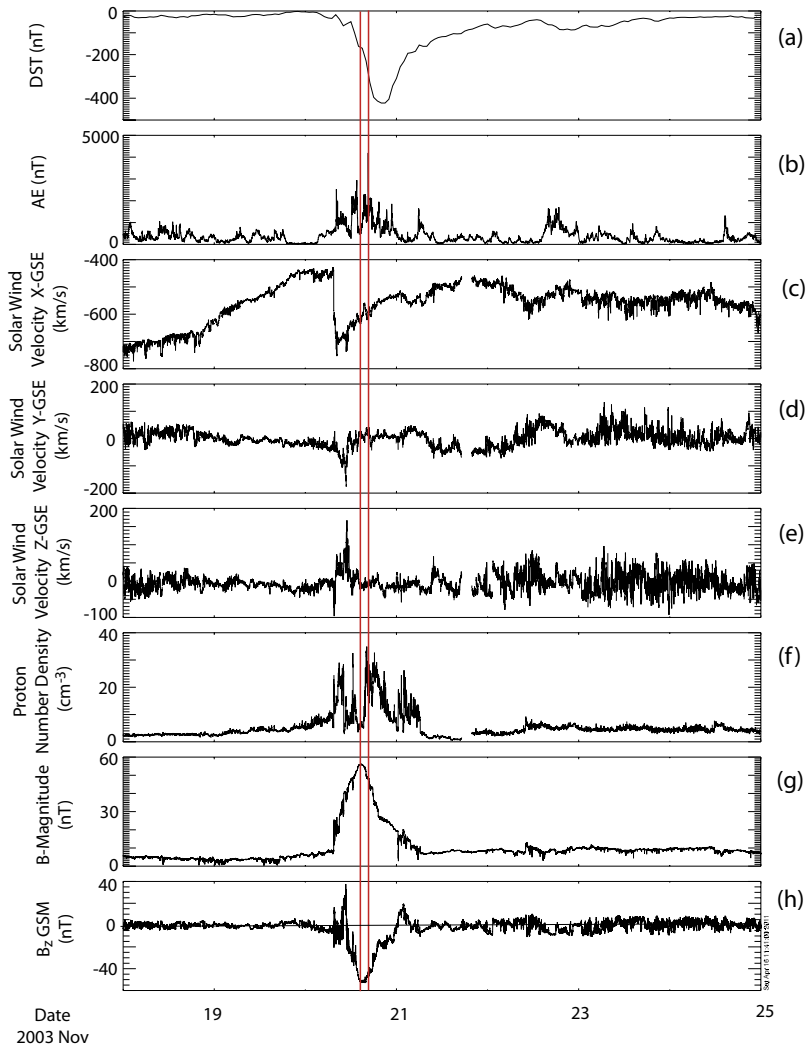

Figure 4.2: Solar wind conditions for the November 2003 storm are presented, including (a) Dst, (b) AE index, (c)-(e) solar wind velocity in GSE coordinates, (f) proton number density, (g) magnetic field magnitude, and (h) magnetic field z-GSM component surrounding the storm. The vertical red bars mark the November 20th pass presented in Chapter 7.

Chapter 5

November 04, 2003 Event

5.1 ACE Data

Before examining the data from Polar, it is necessary to establish the activity level of the event by examining the solar wind conditions, which is done using data from ACE spacecraft. ACE is about 230 R_E sunward of the Earth on November 4th, 2003. Using the x-component of the solar wind velocity, which is around 730km/s during this time, a simple estimate of the propagation time is made by dividing the distance between ACE and the magetopause by the velocity. This yields a propagation time of 33 minutes for the conditions at ACE to reach the magnetopause boundary. The red vertical bars on Figure 5.1 delineate the interval approximately 33 minutes prior to the maximum Poynting flux seen by Polar. The conditions during this time show that the z-component of the magnetic field is between 6-7 nT, which is clearly northward. As discussed in Chapter 2, this will cause reconnection at high latitudes on the night side. Panel (e) of Figure 5.1 also shows a proton bulk flow speed around 755 km/s, which is almost a factor of two larger than quiet conditions.

5.2 Polar Data

Figure 5.2 plots components of the Polar electric and magnetic field data for November 4, 2003 from 14:20-14:22 UT. During this time, Polar is located between -85.7 and -86.4° ILAT, at an MLT of 8.8 and an altitude of 3.5 R_E. Panel (a) shows large fluctuations

in the 1-10s filtered electric field of around 180 mV/m peak-to-peak shortly after 14:21. The magnetic field is also filtered over 1-10s, and fluctuations seen in panel (b) near this time have a peak-to-peak value of about 18 nT. Using these two values yields an E/B ratio of 10,000 km/s, which quite close to the local Alfven velocity of 9,000 km/s. The components of the fields in (a) and (b) are used to calculate one component of the Poynting flux shown in (c), which has peaks in the Poynting flux simultaneous to the electric and magnetic field peaks. To check that the spin-axis electric field does not significantly influence the Poynting flux values, Poynting flux calculated without using the spin-axis electric field is displayed in panel (d). The full Poynting flux presented in (e) has similar structure and magnitude to those in panels (c) and (d), indicating that using the full electric and magnetic field to calculate the full Poynting flux is reasonable for this event. Panel (e) displays a maximum earthward peak at 14:20 of about 50 $ergs/cm^2/s$ when mapped to the ionosphere. If all of this energy were to travel to the ionosphere, it would be much more than the 1 $ergs/cm^2/s$ necessary to power a visible aurora.

Figure 5.3 presents the Hydra particle data for November 4, 2003. Panels (a) through (c) show in-situ full field-aligned Poynting flux filtered over three time scales, and all three have been averaged over 30s to facilitate comparison with the particle kinetic energy fluxes presented in panels (d) and (h). Note that the in-situ Poynting flux values are used here expressly for the purpose of comparison with Hydra particle data. The high-frequency Poynting flux has an Earthward peak of almost 0.1 $erg/cm^2/s$ near 14:10 and 14:21UT, while the medium-frequency peak is roughly a factor of two greater and occurs near 14:21. The low-frequency Poynting flux is substantially greater than the other two, with a peak near 1.2 $erg/cm^2/s$. The electron kinetic energy flux, shown in the fourth panel, peaks at slightly less than 0.2 $ergs/cm^2/s$ near 14:15. The electron energy spectra in panels (e) through (g) show roughly isotropic fluxes for electrons parallel, antiparallel, and perpendicular to the magnetic field, with the exception of some low-energy electrons parallel to the field which are not present in the other two components. The most intense fluxes are present for all three panels at energies of 100 - 1000eV. Panel (h) presents the ion kinetic energy flux, which peaks at around $0.35ergs/cm^2/s$ near 14:20, which is greater than the peak kinetic energy flux of the electrons. The peak in ion kinetic energy is also roughly simultaneous to the

Poynting flux peaks near 14:21. In addition, the ion spectra are clearly anisotropic, as can be seen in the parallel, antiparallel, and perpendicular ion energy spectra in panels (i) through (k). Instead, there is a significant population of high-energy ions with energies between about 10^3 and 10^4 eV in the parallel ions which is not present in the antiparallel ions. This outflow is during Polar crossing into the cusp region beginning around 14:10. Though there is not a traditional cusp signature of inflowing ions, the drop in particle flux near 14:30 indicating open field lines suggests that the spacecraft is crossing the cusp region from closed to open field lines near 14:10. There are also a fairly large population of high-energy ions perpendicular to the field during this time, which may likely be particles from the same population as the upflowing ions which are mirroring at this altitude. In all three spectra, the energy of the ions increases with increasing $|ILAT|$, which is as Polar is moving toward the south pole. This phenomena is consistent with the velocity dispersion expected due to the $\frac{\vec{E}\times\vec{B}}{B^2}$ drift with an eastward electric field resulting from convection toward the dayside.

Field-aligned current structures are characterized by the presence of large magnetic field structures lasting around 20min. which deviate from the direction of the magnetic field line. For a simple current sheet, this would cause a perturbation magnetic field perpendicular to the background field which reverses when crossing through the current sheet; however, the current systems along the field lines tend to be more complex. In the trajectory of Polar through the cusp region during this time, the spin-plane booms were approximately aligned with dipole magnetic field lines as the spacecraft spins, which would imply that the structure should be seen in the 56-component of the magnetic field data. However, due to the distortion of the field during storm conditions, all three components of the field are examined, as shown in Figure 5.4. This data is the "minus model" magnetic field data, such that only the deviations from the field are shown. The 56-component of the field in panel (b) has a bipolar structure lasting roughly 20min. between 14:05 and 14:25 which reaches a peak-to-peak amplitude around 100nT. This is indicative of the presence of a field-aligned current structure during this time, which is the same time interval over which the Poynting flux peaks are seen.

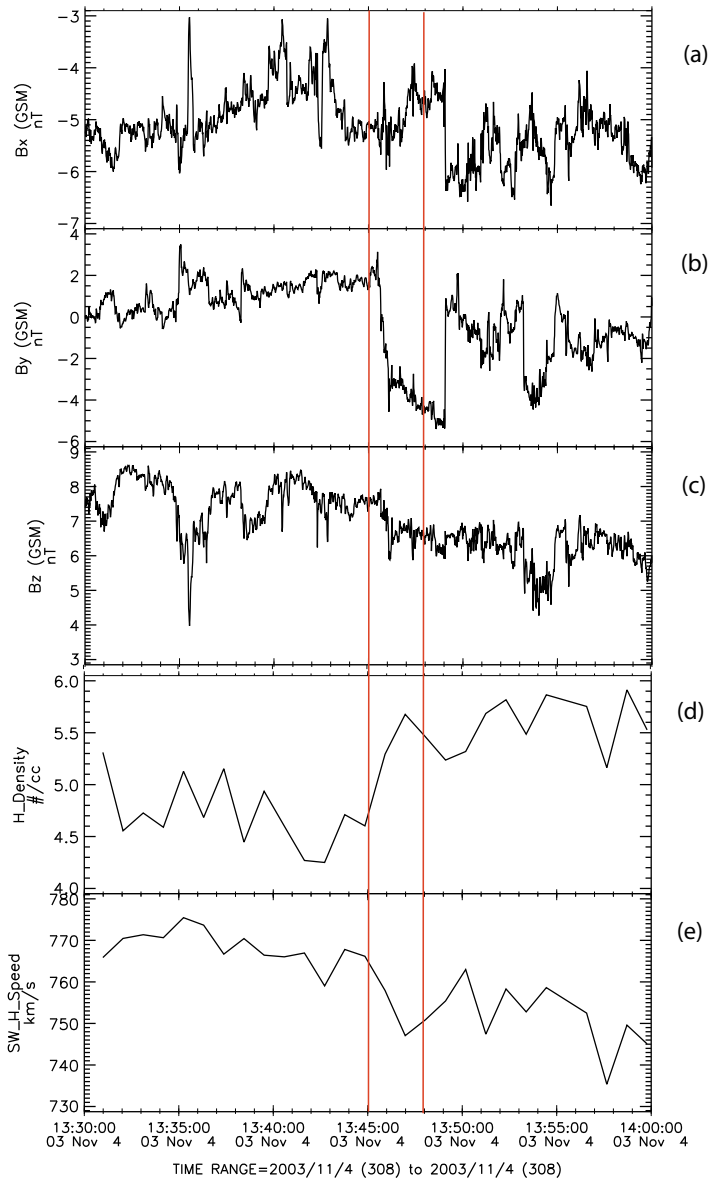

Figure 5.1: Magnetic field data from ACE spacecraft in GSM coordinates is shown in panels (a), (b), and (c), which are the x-, y-, and z-components of the field, respectively. The interval indicated by the red vertical bars shows the IMF conditions which will propagate to Earth at the time that the largest Poynting flux is seen by Polar. The z-component of the magnetic field is clearly northward-pointing during this interval, with an average magnitude around 6.5nT. Panel (d) shows the proton density and panel (e) shows the proton bulk speed.

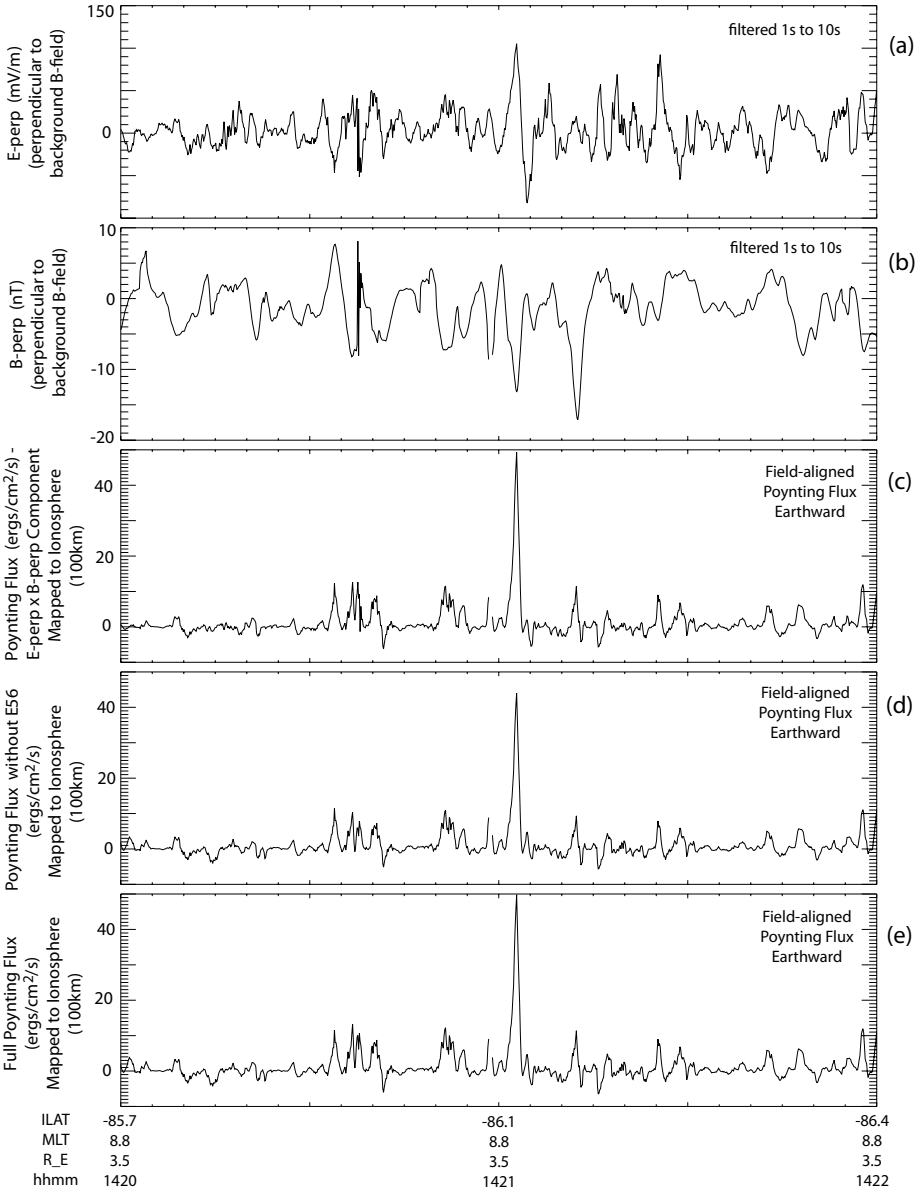

Figure 5.2: Polar electric and magnetic field data was smoothed over 1s and detrended over 10s for this interval. Data displayed includes (a) electric field fluctuations perpendicular to the background magnetic field, (b) the magnetic field fluctuations perpendicular to the background magnetic field, (c) the Poynting flux calculated using these two components, (d) the Poynting flux calculated using only the spin-plane electric field, and (e) the Poynting flux calculated using the full electric and magnetic fields from 14:20 to 14:22UT on November 4, 2003. All Poynting flux data has been mapped to the ionosphere.

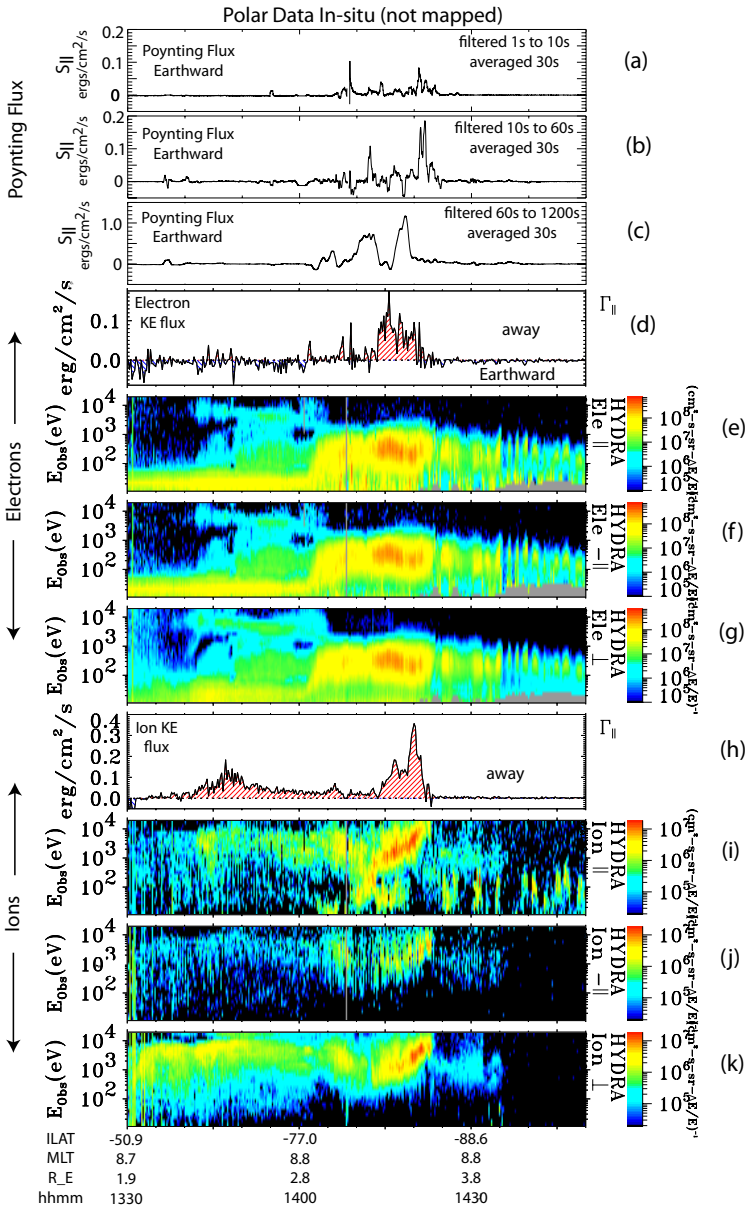

Figure 5.3: Electon and ion data from the Hydra instrument on Polar show peaks in the kinetic energy flux and large populations of high-energy ions simultaneous to the measurement of earthward Poynting flux near 14:20UT on November 4, 2003. The first three panels present Poynting flux (a) filtered 1s to 10s and averaged over 30s, (b) filtered 10s to 60s and averaged over 30s, and (c) filtered 60s to 1200s and averaged over 30s. This is followed by (d) electron kinetic energy flux and electron energy spectra for electrons (e) parallel (0-30°), (f) antiparallel (150-180°), and (g) perpendicular (75-105°) to the magnetic field. The last four panels are the same quantities for ions: (h) kinetic energy flux and ion energy spectra (i) parallel, (j) antiparallel, and (k) perpendicular to the magnetic field.

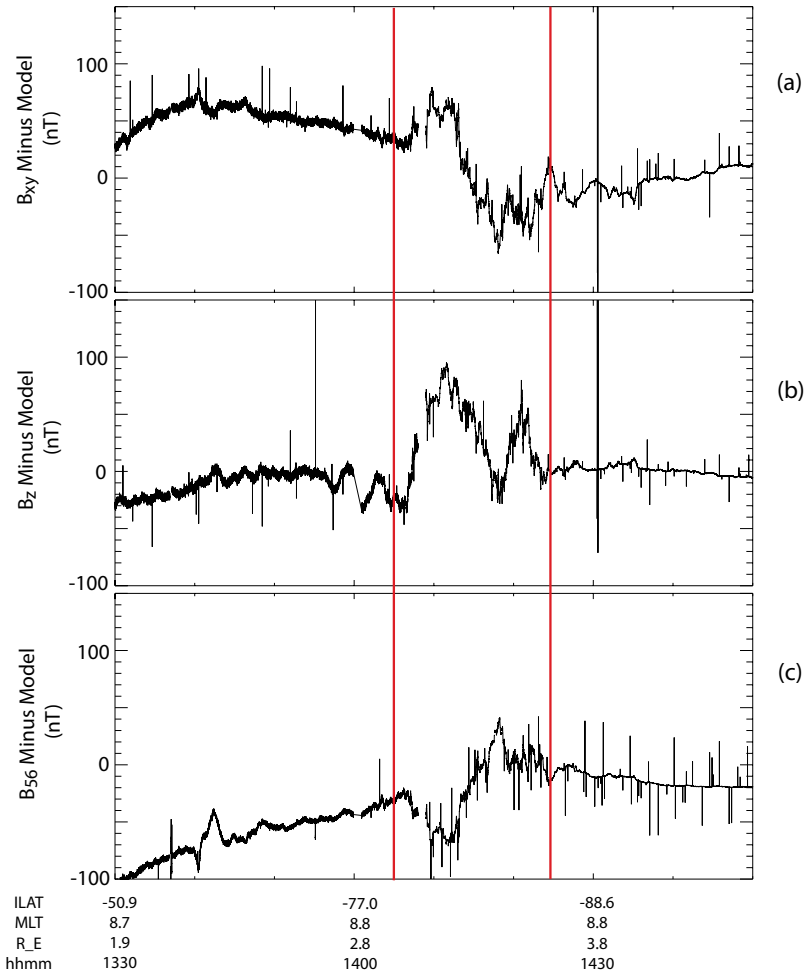

Figure 5.4: The components of the magnetic field minus the model field in spacecraft coordinates, including (a) the xy-component, (b) the z component, and (c) the 56 (spin axis) component for 13:30 through 14:50 UT on November 4, 2003. The vertical red bars delineate a possible field-aligned current signature.

Chapter 6

October 31, 2003 Event

6.1 ACE Data

ACE is roughly 240 R_E sunward of the Earth during the time presented in Figure 6.1. The x-component of the solar wind velocity near 875 km/s leads to an estimate of 28 minutes for the conditions seen by ACE to propagate to the magnetopause. The conditions 28 min previous to when the Poynting flux is seen by Polar are those indicated by the vertical red bars in Figure 6.1. The z-component of the magnetic field during this time is just under 3 nT, which indicates that the field is slightly Northward-pointing. The y-component is of a similar magnitude, at roughly -2nT. The proton bulk speed in panel (e) is around 887 km/s, which is more than a factor of two larger than the velocity during quiet conditions.

6.2 Polar Data

The Polar data presented in Figure 6.2 for 18:02 - 18:10UT on October 31, 2003 shows large electric and magnetic field fluctuations around 18:06-18:07 UT. During this time, Polar is at a distance of 2.8-3.0 R_E, with an ILAT range of -73.5 to -77.4° and an MLT range of 10.0 to 10.4. The electric field fluctuations in panel (a) are as large as 160 mV/m peak-to-peak near 18:06:30, which near the same time as the magnetic field fluctuations in panel (b) with a magnitude of roughly 35nT peak-to-peak near 18:06:20. Using these values to calculate the E/B ratio gives a maximum velocity of about 4500

km/s, which less by about a factor of three than the local Alfven velocity of 12,000km/s (assuming entirely Hydrogen composition). The Poynting flux in panel (c), calculated using the electric field from (a) and the magnetic field from (b), and the Poynting flux calculated with only the spin-plane electric field in (d) are both similar in magnitude and structure to the full Poynting flux in panel (e), which indicates that using the spin-axis electric field in the Poynting flux calculation is valid for this event. Several peaks in the full Poynting flux are also seen at this time in panel (e), with a maximum magnitude of approximately 40 $ergs/cm^2/s$.

The Hydra data for October 31, 2003 is presented in Figure 6.3. As can be seen in panels (a) and (b), both the Poynting flux from fluctuations filtered 1-10s and from fluctuations filtered 10-60s have approximately the same maximum magnitude of roughly 0.17 $ergs/cm^2/s$ when averaged over 30s. Both of these peaks are seen near 18:12UT. The low-frequency (filtered 60s-1200s) Poynting flux peak is almost a factor of 5 larger, as can be seen in panel (c), with a value near 1.0 $ergs/cm^2/s$. Large fluxes of moderate energy electrons (100-1000eV) are present shortly after 18:00 UT, as presented in panels (d) through (f), which appear to be fairly isotropic across all three panels (field-aligned, anti-aligned, and perpendicular), again with a slightly higher population in the field-aligned low-energy electrons. Note that there is no electron kinetic energy flux available for this interval from Hydra. The ion kinetic energy is seen in panel (g), which has a maximum peak of 0.35 $ergs/cm^2/s$ at 18:12. Finally, panels (h) through (j) show the field-aligned, anti-aligned, and perpendicular ion energy fluxes. The field-aligned ion distribution, present shortly after 18:10 when crossing into the cusp region, is quite energetic, with large fluxes between 10^3 and 10^4 eV. These ions also increase in energy as the spacecraft moves poleward. The downgoing fluxes of ions are lower, indicating that there is a substantial energetic upgoing ion population but few downgoing ions. Additionally, there are moderate fluxes of ions perpendicular to the field with similar energies to the upgoing ions.

Examining Figure 6.4 shows that a field-aligned current structure may be present from about 18:03 through 18:17. Though not as clearly structured as for the November 4 event, there is still a clear deviation from the average magnetic field in the 56-component (panel (c)). In this case it seems possible that a substantial amount of the field-aligned current structure is also detected in the z-direction, which peaks near 100nT between

the red bars, as seen in panel (c). This structure is present during the time when the majority of the low-frequency Poynting flux is present.

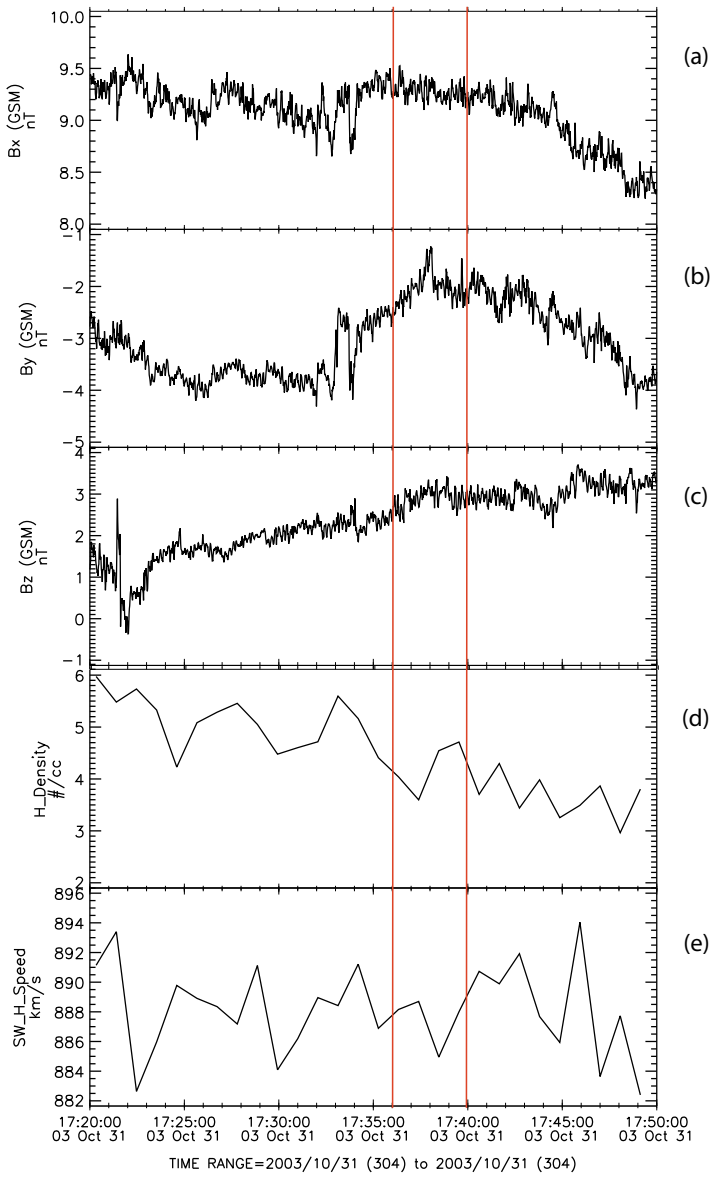

Figure 6.1: Magnetic field data from ACE spacecraft in GSM coordinates (x, y, and z) in panels (a), (b), and (c). Panel (d) shows proton density and panel (e) shows proton bulk speed. The interval indicated by the red vertical bars shows the IMF conditions which will propagate to the earth at the time that the largest Poynting flux is seen by Polar. The z-component of the magnetic field is clearly northward-pointing during this interval, with an average just under 3 nT.

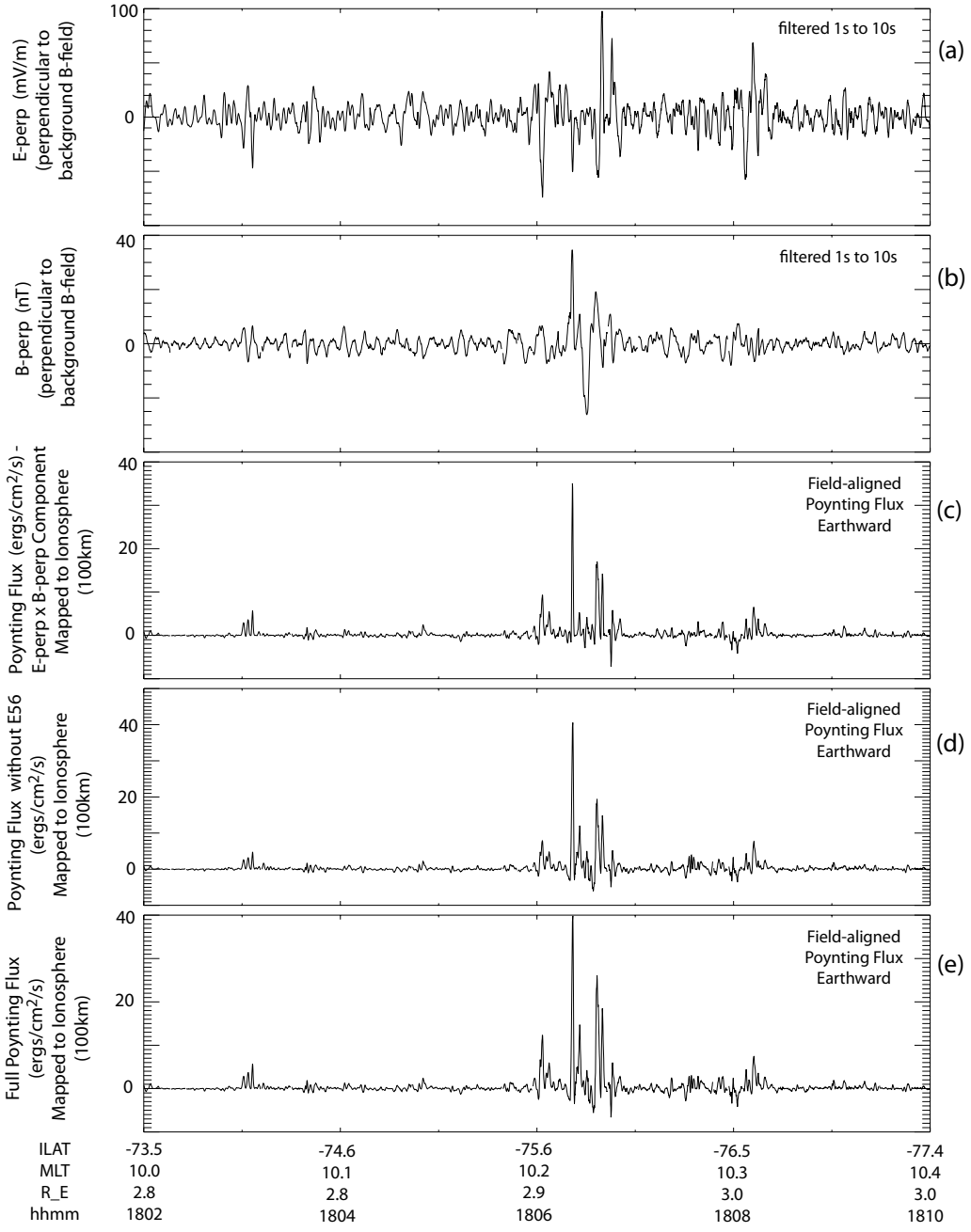

Figure 6.2: Polar electric and magnetic field data smoothed over 1s and detrended over 10s for this interval. Data displayed includes (a) electric field fluctuations perpendicular to the background magnetic field, (b) the magnetic field fluctuations perpendicular to the background magnetic field, (c) the Poynting flux calculated using these two components, (d) the Poynting flux calculated using only the spin-plane electric field, and (e) the Poynting flux calculated using the full electric and magnetic fields from 18:02 to 18:10UT on October 31, 2003. All Poynting flux data has been mapped to the ionosphere.

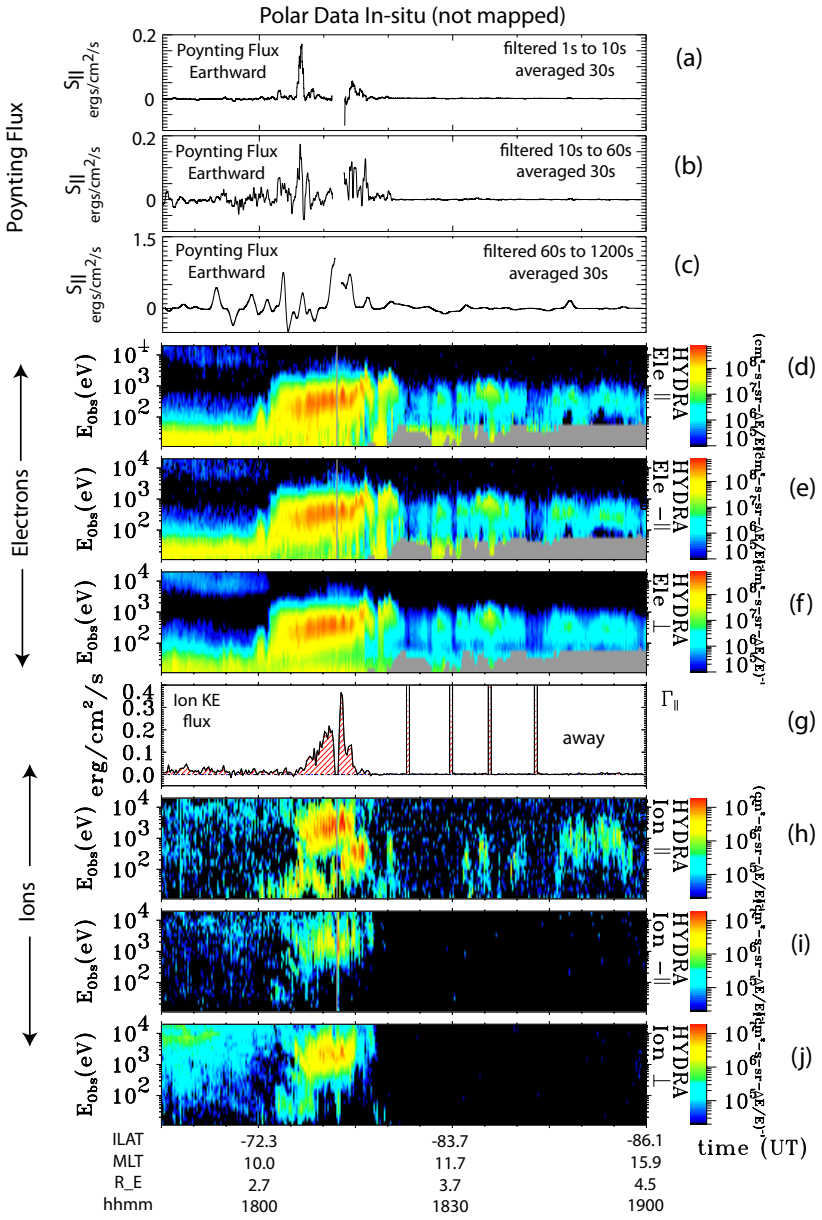

Figure 6.3: Earthward Poynting flux in the frequency ranges 1-10s (a), 10-60s (b), and 60-1200s (c) is presented for the interval from 17:45 through 19:00UT on October 31, 2003. All three Poynting fluxes are also averaged over 30s. Additionally, data from the Hydra instrument provides electron energy spectra for electrons (d) parallel, (e) antiparallel, and (f) perpendicular to the magnetic field. The last four panels show (g) ion kinetic energy flux and ion energy spectra (h) parallel, (i) antiparallel, and (j) perpendicular to the magnetic field.

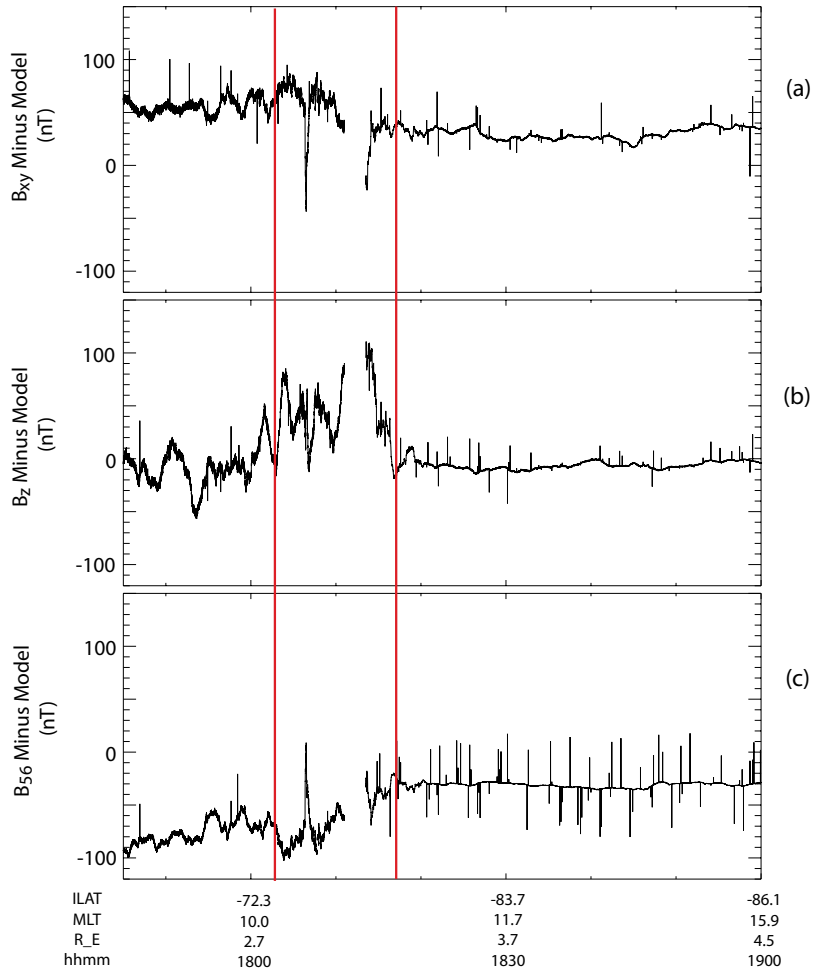

Figure 6.4: The components of the magnetic field minus the model field in spacecraft coordinates, including (a) the xy-component, (b) the z-component, and (c) the 56 (spin axis) component for 17:45 through 19:00 UT on October 31, 2003. The vertical red bars delineate a possible field-aligned current signature.

Chapter 7

November 20, 2003 Data

7.1 ACE Data

Solar wind data from ACE spacecraft is presented in Figure 7.1. ACE is about $250R_E$ sunward of the earth and the x-component of the solar wind velocity is roughly 570km/s during this time, which gives an estimate of about 45min. for the conditions detected by ACE to propagate to the magnetopause. The red vertical bars delineate the conditions at ACE about 45min. before the interval when the most intense Poynting flux is detected by Polar. The IMF has a fairly strong y-component at around 21nT during this period, as seen in panel (b). Of special note, however, is the extremely strong negative z-component of the magnetic field, near -51nT during this time, shown in panel (c). This is unusually strong and stays roughly constant throughout the interval shown. The proton bulk speed in panel (e) is roughly 605 km/s, which is not as high as for the passes during northward IMF, but is still a factor of 1.5 larger than quiet conditions.

7.2 Polar Data

Polar spacecraft electric and magnetic field data for November 20th, 2003 are presented in Figure 7.2. The time interval in which large Poynting flux is seen extends from 15:47-15:52UT, during which Polar is located between -59.3 and -63.9 ILAT and 8.0-8.1 MLT. Panel (a) shows a component of the electric field perpendicular to the background magnetic field, which has been detrended over 10s and smoothed over 1s. The electric

field fluctuations are extremely large during this interval, with the largest being on the order of 240-380 mV/m peak-to-peak. The magnetic field data in panel (b) has been smoothed and detrended over the same scale as the electric field and also shows fluctuations of unusual size, with the largest being on the order of 50-100nT peak-to-peak. Calculating the E/B ratios yield a velocity of 4,750 km/s near 15:47:30 and 2,700 km/s near 15:51, which are around a factor of 5-10 less than the Alfven velocity of 22,000 km/s in this region. Again, this Alfven velocity is calculated assuming entirely Hydrogen composition, which does not account for large populations of heavy ions present during strong storms or the corresponding reduction in Alfven speed. With the presence of such large fluctuations in both the electric and magnetic field, it is not surprising that the Poynting flux calculated using these two components is quite large as well, as shown in panel (c). Both panels (c) and (d) again match well with the full Poynting flux shown in panel (e). The full Poynting flux, when mapped to the ionosphere, has the three largest Poynting flux peaks near 120 $ergs/cm^2/s$ earthward near 15:47:30, -80 $ergs/cm^2/s$ anti-earthward near 15:48:00, and 120 $ergs/cm^2/s$ earthward around 15:51 UT. Such large amounts of Poynting flux are a measure of the intensely active conditions during this interval of the storm.

Figure 7.3 shows the Hydra instrument data for 60 minutes surrounding when the Poynting flux is detected. Panels (a) through (c) show that there is a significant amount of Poynting flux due to high frequency fluctuations (filtered 1s-10s), moderate-frequency fluctuations (filtered 10s-60s), and low frequency fluctuations (filtered 60s-1200s) at approximately the same time as the cusp crossing near 15:50 UT. All scales of Poynting flux were averaged over 30s. Both the high and moderate frequency Poynting flux have Earthward peaks on the order of 0.5 $ergs/cm^2/s$, while the low frequency Poynting flux is significantly larger, with a peak around 9 $ergs/cm^2/s$. The electron kinetic energy flux presented in panel (d) is a similar order of magnitude as the first two panels of Poynting flux, with a peak around 0.4 $ergs/cm^2/s$ anti-Earthward. The ion kinetic energy flux was unfortunately not available during this time interval, as indicated by the absence of panel (h). The field-aligned ions in panel (i) show that there is a large flux of low-energy (70-500eV) ions immediately after Polar has entered the cusp region (or the region with a field-aligned current structure, as discussed in the following paragraph). The ILAT

at this time, calculated using the Tsyganenko 2004 storm-time model to be about -62°, indicates that the cusp location is at an extraordinarily low latitude in comparison with roughly -75° ILAT for the other two events. Only an extreme distortion of the field lines due to the large southward B_z suffices to explain for such an unusual cusp location, which serves as another indicator of the highly active nature of this event, in accord with the large Poynting flux. The anti-aligned ions (panel (j)) do not have the same large fluxes as the aligned ions, which indicates the presence of a low-energy population of ions streaming away from the earth and the absence of any coming in towards the earth. The presence of higher-energy ions (around 10keV) perpendicular to the field, as seen in panel (k) indicates that there may be transverse ion heating occuring at the altitude of Polar, near 2.3 R_E. These ions may also be storm-injected ions mirroring at the altitude of Polar, similar to the population seen by McFadden et al. (2001) [7].

A sharp peak structure is clearly visible in all three components of the minus-model magnetic field, indicating that the 56-axis is probably not entirely perpendicular to the field, as presented in Figure 7.4. This structure lasts for about 10min. from about 15:43 through 15:53 in the 56-component (panel (c)), although it could arguably last closer to 15min. based on the xy- and z-components (panels (a) and (b)). The amplitude of this peak ranges from around 300nT in the 56-component to over 500nT in the z-component. This structure has both a shorter duration and a much larger amplitude than the structures for the other two events, which is likely a result of the extraordinarily strong storm conditions for this event, but may also be indicative of different physics in the current structure. Since the structure is a single peak, it appears that the spacecraft is traversing two current sheets oriented in opposite directions, or a more complex structure with that general form.

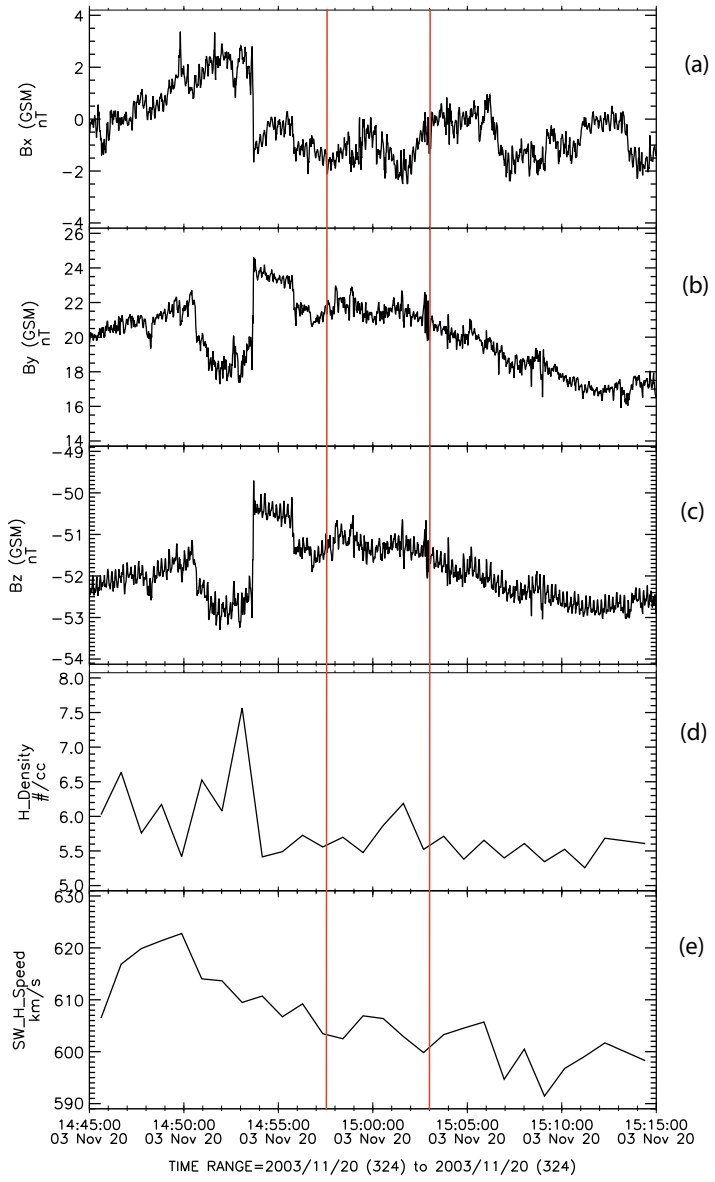

Figure 7.1: Solar wind data from ACE spacecraft in GSM coordinates for the time interval from 14:50 through 16:00UT on November 20, 2003, including (a) x-GSM, (b) y-GSM, and (c) z-gsm. Data for (d) proton density and (e) proton bulk speed are also presented. The interval indicated by the red vertical bars shows the magnetic field conditions which will propagate to the earth at the time that the largest Poynting flux is seen by Polar. The z-component of the magnetic field is clearly southward-pointing during this interval, with a value of around -51nT, which is an order of magnitude larger than the typical B_z component.

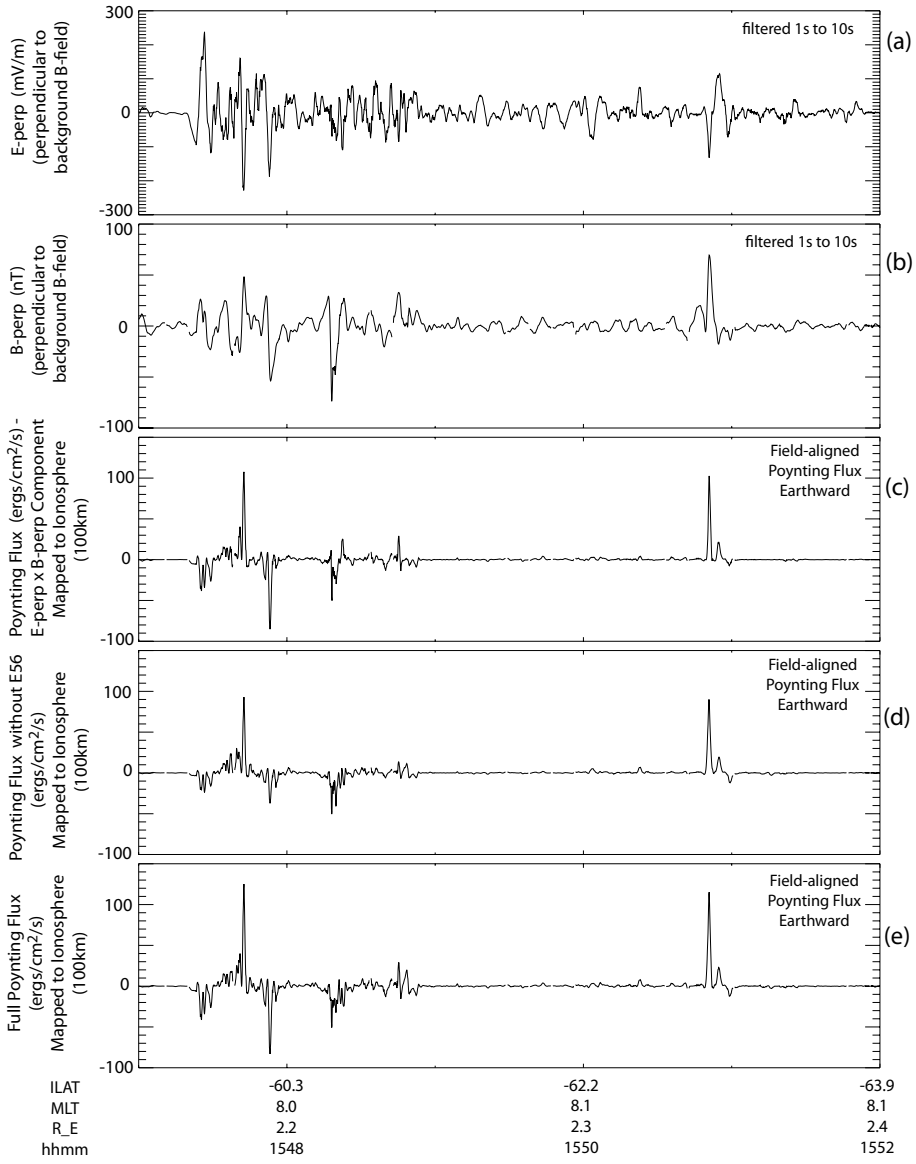

Figure 7.2: Polar data in this figure is smoothed over 1s and detrended over 10s. Data displayed includes (a) electric field fluctuations perpendicular to the background magnetic field, (b) the magnetic field fluctuations perpendicular to the background magnetic field, (c) the Poynting flux calculated using these two components, (d) the Poynting flux calculated using only the spin-plane electric field, and (e) the Poynting flux calculated using the full electric and magnetic fields for the interval 15:47 - 15:52UT on November 20, 2003. All Poynting flux data has been mapped to the ionosphere.

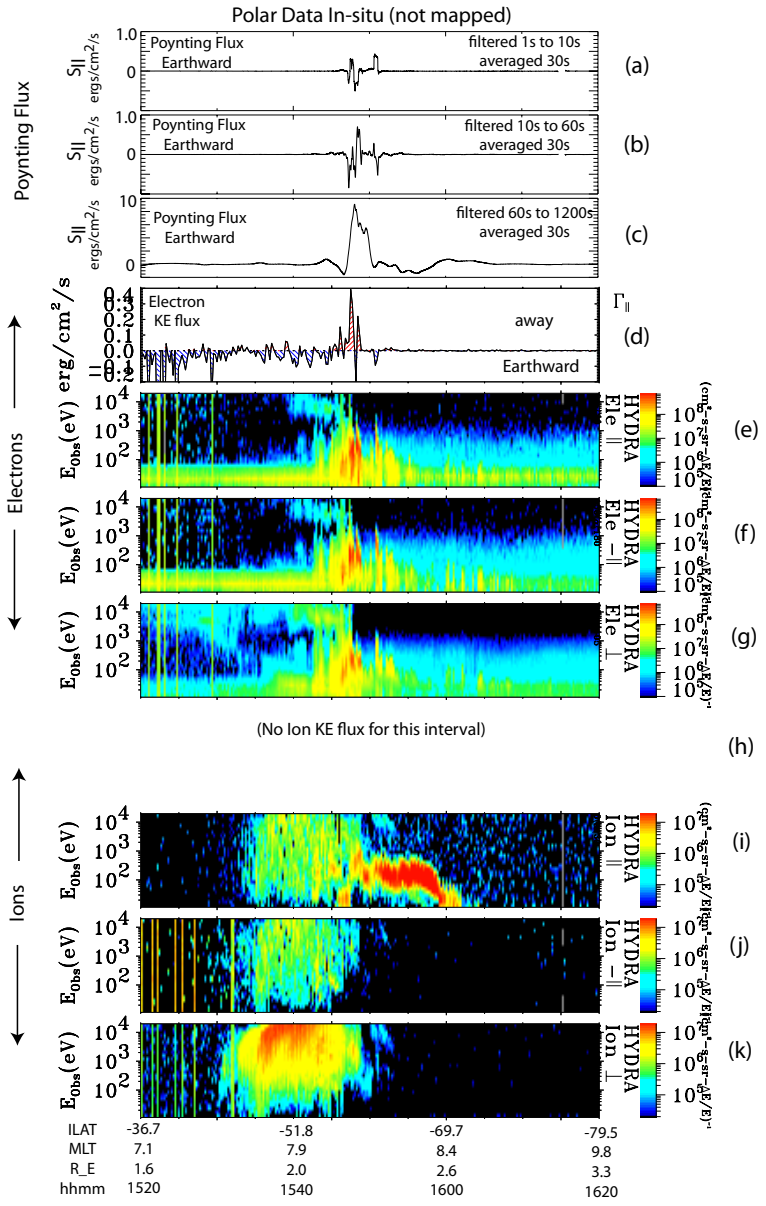

Figure 7.3: Poynting flux filtered over three different intervals for 15:20 - 16:20UT is presented in panels (a) through (c), including Poynting flux (a) filtered 1s to 10s and averaged over 30s , (b) filtered 10s to 60s and averaged over 30s, and (c) filtered 60s to 1200s and averaged over 30s. This is followed by (d) electron kinetic energy flux and electron energy spectra for electrons (e) parallel, (f) antiparallel, and (g) perpendicular to the magnetic field. The last four panels are the same quantities for ions: (h) kinetic energy flux and ion energy spectra (i) parallel, (j) antiparallel, and (k) perpendicular to the magnetic field.

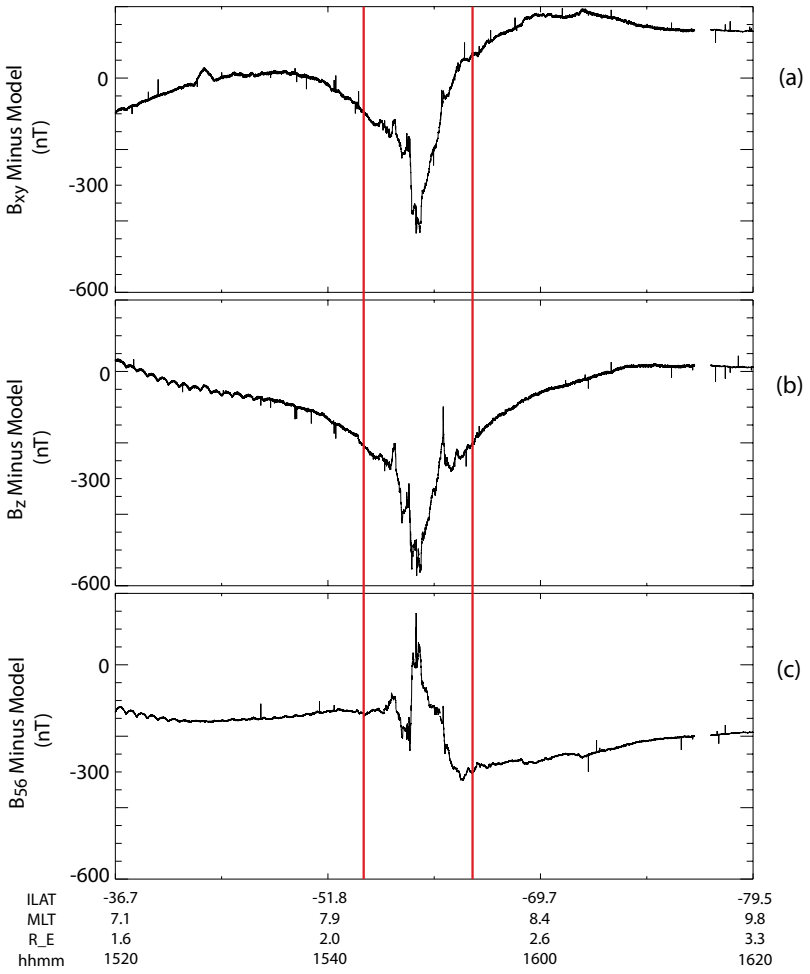

Figure 7.4: The components of the magnetic field minus the model field in spacecraft coordinates, including (a) the xy-component, (b) the z component, and (c) the 56 (spin axis) component for 15:20 through 16:20 UT on November 20, 2003. The vertical red bars delineate a possible field-aligned current signature.

Chapter 8

Analysis and Discussion

In order to assess the energy budget for the events presented, it is useful to compare the magnitude of the Poynting flux with the particle energy for each event, as was done by Chaston et al. (2005) [1]. Beginning with the November 4, 2003 pass, it can be seen in Figure 5.3 that the peak high-frequency (Alfvenic) Poynting flux (0.1 $ergs/cm^2/s$) is not sufficient to account for either the electron kinetic energy flux peak of 0.18 $ergs/cm^2/s$ or the ion kinetic energy flux peak of 0.35 $ergs/cm^2/s$ (note that actual causation is in no way addressed here; this is only a statement of whether the Poynting flux provides enough energy to explain the particle kinetic energy flux peaks). The electron kinetic energy is comparable to the magnitude of the medium Poynting flux (0.2 $ergs/cm^2/s$), so the medium Poynting flux could plausibly provide enough energy to power the electron acceleration. However, the ion kinetic energy must be accounted for as well, and for this event, only the low-frequency Poynting flux associated with the steady-state current structure, with a peak of 1.2 $ergs/cm^2/s$, would provide sufficient energy to accelerate the up-going ions. Summing the peak Poynting fluxes for these frequency bands yield a total of around 1.5 $ergs/cm^2/s$. The peak ion kinetic energy is roughly 20-30% of the total Poynting flux, indicating fairly efficient energy transfer from the Poynting flux into powering ion acceleration.

For the October 31, 2003 pass, the high- and medium-frequency Poynting fluxes are comparable to those in the November 4 pass, in this case both peaking around 0.17 $ergs/cm^2/s$. The low-frequency Poynting flux is somewhat smaller than for November 4, around 1.0 $ergs/cm^2/s$. As with November 4th, only the low-frequency Poynting

flux provides sufficient energy in this region to account for the ion kinetic energy flux peak of 0.37 $ergs/cm^2/s$. Unfortunately, the lack of electron kinetic energy flux data prevents a full assessment of the energy balance for this event. The total Poynting flux is of similar magnitude to November 4, at around 1.34 $ergs/cm^2/s$, and again the peak ion kinetic energy flux is 20-30% of the total Poynting flux.

On November 20, 2003 the low-frequency Poynting flux is nearly a factor of 20 greater than the high- and medium-frequency Poynting fluxes. The high-frequency Poynting flux has a peak of roughly 0.4 $ergs/cm^2/s$, while the medium is slightly larger, around 0.7 $ergs/cm^2/s$. In contrast, the low-frequency Poynting flux associated with the field-aligned current system is around 9.0 $ergs/cm^2/s$, which is nearly an order of magnitude larger than the low-frequency Poynting flux for the passes during northward IMF. However, this may also be influenced by the fact that this pass is at lower altitude than the November 4 and October 31 passes. Since the IMF is strongly southward during this interval, it seems reasonable to assume that the increased intensity of reconnection would cause larger deviations from the background magnetic field to be present in the field-aligned current system, which is consistent with the substantial magnitude of this large-scale Poynting flux. For this event, the electron kinetic energy flux is around 0.4 $ergs/cm^2/s$, which is less than or equal to the energy provided by any of the three frequency bands of Poynting flux, such that any of them could possibly provide enough energy to power the electrons. Total in-situ Poynting flux for this pass is roughly 10.1 $ergs/cm^2/s$, again roughly a factor of 10 greater than for the northward IMF passes. Though there is no ion kinetic energy flux present for this event, comparison with the November 3 pass during southward IMF, which has a similarly-large low-frequency Poynting flux peak of 7.5 $ergs/cm^2/s$ and an ion kinetic energy flux peak of 0.05 $ergs/cm^2/s$, suggests that the efficiency of the ion acceleration is less for southward events.

From the six events analyzed for this study (three of which were selected due to their structured ion spectra), the Hydra plots consistently show a population of upgoing ions with energies above 1000 eV for northward IMF. In addition to the data presented for November 4 and October 31, the event on November 23, 2003 has an IMF z-component of about 5 nT and shows a similarly-structured field-aligned ion spectra to that for November 4th. Events with southward IMF tended to have larger fluxes of field-aligned

ions at lower energies. Data for November 3, 2003 has a very localized population of ions with energies less than 100eV present during an IMF of about -1.5 nT. October 29, 2003 lacked ACE data to determine the direction of the IMF; instead, Omni data was used to estimate the IMF for that time to be northward. However, the October 23 pass has multiple intense patches of ions less than 1000eV which look quite similar to the data presented for November 20 in Figure 7.3, such that northward IMF is questionable. Based on the similarity of structures in the upgoing ions with November 20, it is suggested that the October 29 event is likely during southward IMF.

The significant fluxes of upgoing ions in these events allows for comparison with previous research on upgoing ions. For the November 4 event, the ratio between the ion and electron kinetic energies is drastically different than that presented in Wygant et al. (2000). In that work, the outflowing ions only had energies around several percent of the electron energy, whereas in this case the ion kinetic energy exceeds that of the electrons by roughly a factor of two. However, this difference may be a result of taking data from very different locations, since their data was taken with Polar spacecraft at a higher altitude (4-6 R_E), on the night side, and on field lines mapping to the auroral zone [8]. Additionally, their measurements were for downgoing electrons, suggesting that there is something different about the Poynting flux dissipation and particle energization in the dayside cusp such that the ratio of ion energy to electron energy is significantly larger than in the 2000 study.

Lockwood et al. (1998) presents instances of downgoing and mirrored (upgoing) ions with discrete step in flux present in the energy spectra, which is suggested to be a signature of pulsed reconnection. The upgoing ion energy spectrum for October 31 has a large flux of ions between 10^3 and 10^4 eV in the interval from 18:10 to 18:20, which is followed by a shorter interval of ion flux with energies in the range of 10^2 to 10^3 eV. Though there is some overlap in the time that these two populations are present, going from the first to the second population does exhibit a downward step in energy, similar to that presented by Lockwood et al. (1998). This step is not as clearly defined as those presented in that study, but may still be indicative of a pulsed reconnection process mapping to the cusp [10].

The two northward IMF events presented (Chapters 5 and 6) and the November 23, 2003 event clearly all show ions increasing in energy with increasing ILAT, i.e. as

Polar moves toward the cusp. This is consistent with $\frac{\vec{E}\times\vec{B}}{B^2}$ drift due to the convection electric field associated with field lines convecting toward the dayside, as expected for northward IMF. The phenomena is also mentioned in Cargill et al. 2005 as a reversed dispersion signature which is related to reconnection occurring in the lobe rather than in the subsolar region [12]. In contrast, the events with Southward IMF do not have the clear increase in ion energy with latitude in the field-aligned ions. Instead, the events analyzed show very intense patches of lower energy ions with energies that either stay relatively constant or decrease with increasing ILAT.

The three events shown are clearly in accord with Strangeway et al. (2005), Zheng et al. (2005), and Burchill et al. (2010) in that both Poynting flux and low-energy electrons are present simultaneous to upflowing ions [13], [15], [6]. The electron spectra for both October 31 and November 4 both have slightly larger fluxes of 10eV to 100eV electrons in the parallel spectra than in either the antiparallel or perpendicular spectra, which suggests that there are also low energy electrons present simultaneous to the upgoing ions. However, this analysis is slightly different from those studies in that the low-energy electron population for these events is seen in the upgoing electrons rather than the downgoing electrons. Poynting flux is quite clearly present for all three events, and is present in large quantities associated with the field-aligned current system. The Poynting flux presented here, however, also differs from the other studies in frequency band; Strangeway et al. (2005) used data with periods longer than 4s, and Zheng et al. (2005) used data with periods between 6s and 600s. The electron kinetic energy flux presented here indicates that the energy from any precipitating electrons is completely dominated by upflowing electrons, suggesting that in this case Poynting flux is the dominant energy input for powering the acceleration of upflowing ions.

Of the different energy forms discussed in Chapter 2, the lack of large fluxes of downgoing ions in the Hydra data suggest that ion jets streaming from the reconnection region along the field lines are not one of the main energy sources present, or at least that the field lines which Polar is traversing are not connected to the X-line. It is also likely that these ion jets are mirroring at an altitude above Polar. Alfven waves are detected for all three events, indicating that the high-frequency Poynting flux is Alfvenic; it is also one of the significant energy sources in the dayside cusp region. In addition, low-frequency Poynting flux associated with the field-aligned current system

Date	Time (UT)	IMF	High $S_{\parallel}$ ($\frac{ergs}{cm^2 sec}$)	Medium $S_{\parallel}$ ($\frac{ergs}{cm^2 sec}$)	Low $S_{\parallel}$ ($\frac{ergs}{cm^2 sec}$)	Ion KE Flux ($\frac{ergs}{cm^2 sec}$)	Electron KE Flux ($\frac{ergs}{cm^2 sec}$)	$E_{\perp}$
10/31	18:07	N	0.17	0.17	1.0	0.37	n/a	Y
11/04	14:21	N	0.1	0.2	1.2	0.35	0.18	Y
11/23	17:40	N	0.04	0.1	0.95	n/a	0.08	Y
10/29	10:57	?N	-0.07	-0.13	-1.7	0.7	n/a	Y
11/03	00:51	S	1.3	1.3	7.5	0.05	-0.3	Y
11/20	15:47-52	S	0.4	0.7	9.0	n/a	0.4	Y

Table 8.1: All events listed are in 2003. Table (above) shows the energy flux from different sources for the events analyzed. Note that the Poynting flux amounts are all in-situ values for high (filtered 1-10s), medium (filtered 10-60s), and low (filtered 60-1200s) frequency Poynting flux which have been averaged over 30s. Kinetic energy flux values are not available for both particles for all events, as indicated by (n/a) in the table. The presence of energetic particle populations perpendicular to the field is either marked as present or not (Y/N) in the table above.

contributes a substantial amount of energy. For all three events presented, there is also a population of high-energy ions present perpendicular to the field lines, which suggests that some of the ions are being transversely accelerated at the same altitude as Polar, or possibly mirroring at the same altitude. Whether the transverse acceleration is due to ion cyclotron waves or kinetic Alfven waves will be an area for further study.

A summary of the energy budget present for each of the events analyzed can be seen in Table 8.

Chapter 9

Conclusion

In sum, there are a variety of energy forms present in the intermediate-altitude cusp region at low altidude on the Earth's day side during strong geomagnetic storms over intervals with both northward and southward IMF. The analysis presented herein has shown that, of the energy sources listed at the beginning of this paper, there is reasonable support to believe that high-frequency (Alfvenic) Poynting flux, Poynting flux associated with field-aligned current structures, and intermediate-frequency Poynting flux are the dominant energy sources used to power the acceleration of particles in the intermediate altitude cusp region. Note that energy from inflowing ion jets from the reconnection region is not detected by Polar during these passes, indicating that these particles have likely mirrored above the altitude of Polar. Instead, fluxes of upflowing ions and electrons are detected on the same magnetic field lines as the Poynting flux, and it has been shown that there is a sufficient amount of Poynting flux present at this altitude to account for the kinetic energy flux of both the electrons and ions. The instances presented show that typically the energy from the high frequency Poynting flux (filtered 1-10s) is less than or roughly equal to the energy from the medium frequency Poynting flux (filtered 10-60s), and that the energy of the low frequency Poynting flux (filtered 60-1200s) is greater than either of the other two frequency bands, often by a factor of 5 or more. In the passes during northward IMF, only the low-frequency Poynting flux provides sufficient energy to account for the peak ion kinetic energy flux. For the November 4 and October 31 passes, the ion kinetic energy is roughly 20-30% of the total Poynting flux, indicating that the particle acceleration processes at this altitude

have a substantial efficiency. Though there is more Poynting flux detected during the passes with southward IMF, the efficiency of energizing ions appears to be lower than during passes with northward IMF. The data suggests that the energy needed to power the high-energy upflowing ions detected during northward IMF is provided by the low-frequency Poynting flux associated with the field-aligned current system, but a more comprehensive study would be necessary to support this.

References

[1] C. C. Chaston. Energy deposition by Alfven waves into the dayside auroral oval: Cluster and FAST observations. *Journal of Geophysical Research*, 110, 2005.

[2] J.W. Dungey. Interplanetary magnetic field and the auroral zones. *Physical Review Letters*, 6(2):47–48, 1961.

[3] C. C. Chaston et al. Auroral ion acceleration in dispersive Alfven waves. *Journal of Geophysical Research*, 109, 2004.

[4] C.T. Russell et al. The GGS/Polar magnetic fields investigation. *Space Science Reviews*, 71:563–582, 1995.

[5] E.C. Stone et. al. The Advanced Composition Explorer. *Space Science Reviews*, 86:1–22, 1998.

[6] J. K. Burchill et al. Thermal ion upflow in the cusp ionosphere and its dependence on soft electron energy flux. *Journal of Geophysical Research*, 115, 2010.

[7] J. P. McFadden et al. FAST observations of ion outflow associated with magnetic storms. *Space Weather, Geophys. Monogr. Ser.*, 125:413–421, 2001.

[8] J.R. Wygant et al. Polar spacecraft based comparisons of intense electric fields and Poynting flux near and within the plasma sheet-tail lobe boundary to UVI images: An energy source for the aurora. *Journal of Geophysical Research*, 105(A8):18675–18692, 2000.

[9] J.Scudder et al. Hydra - A 3-dimensional electron and ion hot plasma instrument for the Polar spacecraft of the GGS mission. *Space Science Reviews*, 71:459–495, 1995.

[10] M. Lockwood et al. Modelling signatures of pulsed magnetopause reconnection in cusp ion dispersion signatures seen at middle altitudes. *Geophysical Research Letters*, 25:591–594, 1998.

[11] P. Harvey et al. The electric field instrument on the Polar satellite. *Space Science Reviews*, 71:583–596, 1995.

[12] P.J. Cargill et al. Cluster at the magnetospheric cusps. *Space Science Reviews*, 118:321–366, 2005.

[13] R.J. Strangeway et al. Factors controlling ionospheric outflows observed at intermediate altitudes. *Journal of Geophysical Research*, 110, 2005.

[14] T. E. Moore et al. Ionospheric mass ejection in response to a CME. *Geophysical Research Letters*, 26:2339–2342, 1999.

[15] Y Zheng. et al. Polar study of ionospheric ion outflow versus energy input. *Journal of Geophysical Research*, 110, 2005.

[16] R. Harten and K. Clark. The design features of the GGS Wind and Polar spacecraft. *Space Science Reviews*, 71:23–40, 1995.

[17] M. Kivelson and C.T. Russell, editors. *Introduction to Space Physics*. Cambridge University Press, New York, NY, 1997.

[18] M.F. Smith and M. Lockwood. Earth's magnetic cusps. *Reviews of Geophysics*, 34(2):233–260, 1996.

[19] S.S. Suess and B. T. Tsurutani, editors. *From the Sun: Auroras, Magnetic Storms, Solar Flares, Cosmic Rays*. American Geophysical Union, Washington, D.C., 1998.

[20] N.A. Tsyganenko and M.I. Sitnov. Modeling the dynamics of the inner magnetosphere during strong geomagnetic storms. *Journal of Geophysical Research*, 110, 2005.

Appendix A

Glossary and Acronyms

Care has been taken in this thesis to minimize the use of jargon and acronyms, but this cannot always be achieved. This appendix defines jargon terms in a glossary, and contains a table of acronyms and their meaning.

A.1 Glossary

- **Bow Shock** – The shock formed sunward of the Earth due to the interaction between the magnetosphere and the solar wind. [19]
- **Coronal Mass Ejection** (**CME**) – A plasma blob flowing from the outer solar atmosphere (corona). [19]
- **Cusp** – The region between the closed magnetic field lines on the sunward side of the Earth and those opening to the solar wind, located about 15° equatorward of the poles. [19]
- **Disturbance Storm Time Index** (**Dst**) – This index uses variations in the Earth's ring current to gauge the activity level of the magnetosphere. [19]
- **Ecliptic plane** – The plane of the orbit of the Earth around the Sun. [19]
- **Frozen-in Condition** – An approximation in which the magnetic field lines in a plasma move with the plasma particles, as though they were frozen in to a volume of plasma. [19]

- **Geomagnetic Storm** – Magnetospheric activity such that the Dst index reaches -50 nT or below. [19]
- **Interplanetary Magnetic Field** (**IMF**) – The magnetic field present in space between planets, caused by the magnetic field frozen in to the plasma flowing off of the Sun. [19]
- **Ionosphere** – A region of the Earth's upper atmosphere composed of free electrons and ions. [19]
- **Invariant Latitude** (**ILAT**) – Latitude as defined by the position at which a field lines reaches the surface of the Earth. [17]
- **L-shell** – A measurement of the distance from the equator at which a given field line crosses the equatorial plane. [17]
- **Magnetic Local Time** (**MLT**) – Time defined based on the position of a given location relative to the sun, with noon pointing directly toward the sun and midnight pointing directly away from the sun.
- **Magnetic Reconnection** – Simplistically, when oppositely-directed field lines become interconnected and change configuration. [19]
- **Magnetopause** – The boundary formed due to balanced pressure of the solar wind and the magnetosphere. [19]
- **Magnetosheath** – The area between the bow shock and the magnetopause containing turbulent plasma. [19]
- **Magnetosphere** – Interaction of the solar wind and the Earth's magnetic field causes the formation of this 'bubble' around the Earth into which the solar wind cannot penetrate. [19]
- **Plasma** – Ionized gas which exibhits collective behavior, but is composed of equal numbers of electrons and ions such that it is neutral overall. [19]
- **Radiation Belt** – Regions near the Earth (1.2-6R_E) in which the magnetic field traps charged particles. [19]

- **Ring Current** – A current around the Earth due to electrons and ions in the earth's magnetic field drifting in opposite directions around the earth, due to the conservation of the third adiabatic invariant. [17]
- **Solar Wind** – Particles (in a plasma state) and magnetic field streaming off of the Sun and into space. [19]

A.2 Acronyms

Table A.1: Acronyms

Acronym	Meaning
ACE	Advanced Composition Explorer (spacecraft)
CME	Coronal Mass Ejection
Dst	Disturbance Storm Time (Index)
ILAT	Invariant Latitude
MLT	Magnetic Local Time
R_E	Earth Radii
Ts04s	Tsyganenko 2004 storm time model